EES Catalysis

REVIEW ARTICLE

View Article Online
View Journal | View Issue

Cite this: *EES Catal.*, 2023, 1, 434

Received 22nd March 2023,
Accepted 21st May 2023

DOI: 10.1039/d3ey00063j

rsc.li/eescatalysis

Single-site catalysts for CO_2 electroreduction

Wenzhong Huang,†[a] Jiexin Zhu,†[a] Shanlin Liu,†[a] Wei Zhang,[a] Liang Zhou *[abc] and Liqiang Mai *[abc]

The use of electrocatalytic carbon dioxide reduction (ECR) for producing various high-value-added products is critical for achieving carbon neutrality. In the past decades, single-site catalysts (SSCs), such as single-atom catalysts, homogeneous molecular catalysts, metal–organic-framework-supported and covalent-organic-framework-supported SSCs, have shown good selectivity and activity for ECR. In this review, we systematically discuss the design principles and optimization strategies for ECR SSCs, starting with the reaction mechanism and descriptors of ECR. We highlight representative studies conducted in the past decades to elucidate the selectivity and reaction mechanisms of different types of SCCs for ECR. Finally, we describe the remaining challenges and perspectives in the application of these emerging catalysts.

Broader context

Excessive fuel combustion and greenhouse gas emission lead to global environmental deterioration. By converting carbon dioxide into valued chemicals and fuels, electrocatalytic carbon dioxide reduction (ECR) is of great significance to alleviate the environmental issue. However, ECR electrocatalysts suffer from limited activity, low selectivity, and unsatisfactory stability. As a result, developing efficient, stable, and low-cost ECR catalysts is of vital importance. Recently, single-site catalysts (SSCs) have emerged as promising ECR catalysts due to their precisely controllable structure and high atomic utilization efficiency. Herein, to accelerate the development of SSCs for ECR, it is necessary to summarize their recent progress on design principles and optimization strategies. This review shows how SSCs are one of most promising candidates for ECR based on latest studies. The researches on these emerging SSCs for ECR have also been comprehensively summarized and discussed, including their catalytic mechanisms, synthesis, optimization strategies, remaining challenges and perspectives. We hope to provide a comprehensive overview of state-of-art progress to readers and shed light on this important field.

[a] *State Key Laboratory of Advanced Technology for Materials Synthesis and Processing, Wuhan University of Technology, Wuhan 430070, Hubei, P. R. China. E-mail: mlq518@whut.edu.cn, liangzhou@whut.edu.cn*
[b] *Hubei Longzhong Laboratory, Wuhan University of Technology (Xiangyang Demonstration Zone), Xiangyang 441000, Hubei, P. R. China*
[c] *Hainan Institute, Wuhan University of Technology, Sanya 572000, Hainan, P. R. China*
† W. H., J. Z. and S. L. contributed equally to this work.

Wenzhong Huang

Wenzhong Huang received his BS degree in Material Science and Engineering from Wuhan University of Technology in 2017. He is currently working toward the PhD degree and his current research focuses on catalysts for electrocatalytic carbon dioxide reduction, water splitting, and anode materials for lithium metal battery.

Liang Zhou

Liang Zhou received his Bachelor (2006) and PhD (2011) degrees from Fudan University under the supervision of Prof. Dongyuan Zhao and Prof. Chengzhong Yu. After graduation, he joined Nanyang Technological University as a Research Fellow in 2011 (with Prof. Xiong Wen Lou) and the University of Queensland as a Postdoctoral Research Fellow in 2012 (with Prof. Chengzhong Yu). He joined Wuhan University of Technology as a full professor in 2015. His research interests include functional nanomaterials for electrochemical energy storage.

1. Introduction

Because of industrial development and the progress of society, a large amount of carbon dioxide (CO_2) is emitted into the air, causing the greenhouse effect. Therefore, the recovery of CO_2 is important for mitigating the current crisis. In particular, electrocatalytic carbon dioxide reduction (ECR) produces C_1, C_2, and C_{2+} products (such as carbon monoxide, ethanol, and dimethyl carbonate) with industrial value and promotes the carbon cycle of the natural environment.[1–4] However, the high-energy barrier to activate the stable CO_2 molecules makes ECR full of challenges.[5–7] In addition, the large-scale application of ECR often suffers from limitations such as limited activity, low selectivity, and unsatisfactory stability. Thus, designing and developing catalysts with satisfactory ECR performance is of great significance.

Since Hori's pioneering research in the 1980s,[8] metals and alloys have been extensively investigated for ECR applications. In recent decades, single-site catalysts (SSCs) have emerged as a new type of catalyst because of their precisely controllable structure and high atomic utilization efficiency.[9–16] The SSCs with active metal center isolated by non-metal atoms mainly contain single-atom catalysts (SACs),[17,18] homogeneous molecular catalysts (HMCs),[19,20] as well as metal organic framework-supported (MOF-supported)[21,22] and covalent organic framework-supported (COF-supported) SSCs.[23,24] The unique coordination environment of SSCs paves a new way for regulating the intrinsic charge, spinning order, and charge transfer of catalysts. Furthermore, the unique coordination structure with a single metal center isolated by non-metal atoms effectively suppresses the competing hydrogen evolution reaction (HER). In addition, the controllable structure of SSCs is also beneficial for the structural design of catalyst, study of reaction mechanism, and evolution of reaction products during the ECR reaction.[14,25–27] Numerous theoretical and experimental studies have demonstrated the application potential of SSCs in ECR.[28–31]

In this review, we comprehensively summarize the researches on these emerging SSCs for ECR, including their catalytic mechanisms, synthesis, optimization strategies, and remaining challenges. Furthermore, we introduce the fundamental ECR reaction mechanism and reaction descriptors to better understand and study the design and reaction mechanisms of different catalysts. We describe recent representative studies on SACs (such as carbon-based and MOF-derived), HMCs (such as phthalocyanine, porphyrin, dipyridine, and their derivatives), MOF-supported SSCs (located in different parts of MOFs) and COF-supported SSCs (such as imine-based and amine-based) to elaborate the advantages and disadvantages of SSCs for ECR (Fig. 1). Finally, we discuss the opportunities and perspectives in the application of these emerging SSCs.

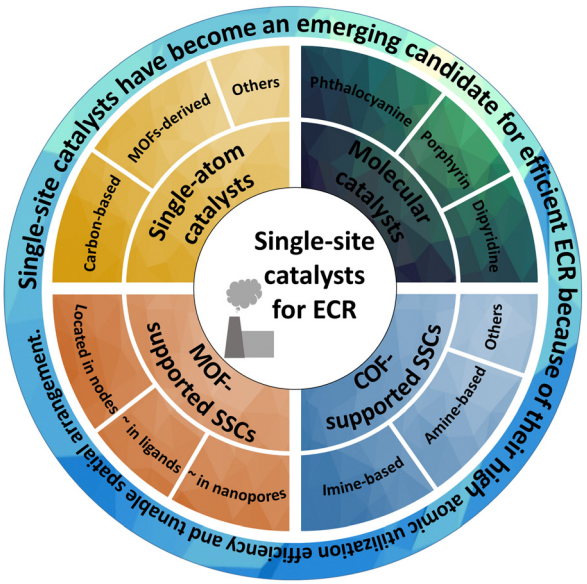

Fig. 1 Various SSCs for ECR, including SACs, HMCs, MOF-supported SSCs, and COF-supported SSCs *etc.*

Liqiang Mai

Liqiang Mai is a Chair Professor of Materials Science and Engineering at the Wuhan University of Technology (WUT), Dean of the School of Materials Science and Engineering at WUT, and Fellow of the Royal Society of Chemistry. He received his PhD from WUT in 2004 and carried out his postdoctoral research at Georgia Institute of Technology in 2006–2007. He worked as an advanced research scholar at Harvard University in 2008–2011 and the University of California, Berkeley in 2017. His current research interests are focused on new nanomaterials for electrochemical energy storage and micro/nano energy devices.

2. Fundamental mechanisms of ECR

2.1. Reaction processes of ECR and catalyst selectivity

ECR is a highly intricate reaction that involves a proton-coupled multi-electron transfer process, and a wide range of products can be generated under different conditions (Fig. 2). Take reactors for example, H-cell are widely used in laboratory investigations but limited to low CO_2 solubility. To overcome these limitations, flow cell with gas diffusion electrode (GDE) to improve local CO_2 concentration have been implemented. However, the GDE is easy to be flooded during long-term operation. Therefore, zero-gap membrane electrode assembly reactor has been applied to overcome flooding. Besides, the electrolyte (solid/liquid electrolyte, anion/cation species, pH, *etc.*) and cell design (ion exchange membranes, pressure, temperature, *etc.*) should also be considered, because of their significant impacts on product reaction and selectivity.[32]

Half-reactions with major reported products are outlined here, without considering the reaction conditions.[33] Unless stated otherwise, all potentials in this study are *versus* the reversible hydrogen electrode (RHE).

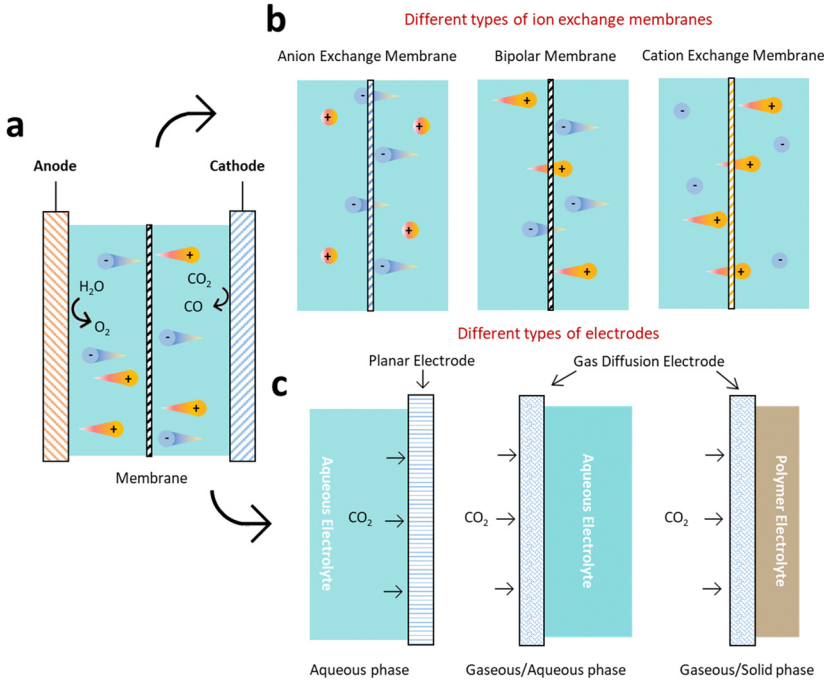

Fig. 2 Schematic diagram of ECR device and influencing factors. (a) A typical ECR system. The anodic and cathodic electrocatalysts perform oxidation and reduction reactions, respectively. (b) The membrane separates the cathodic and anodic compartments. (c) Three different types of electrodes for ECR.

$$CO_2 + 2H^+ + 2e^- \rightarrow CO + H_2O \quad E^0 = -0.10 \textit{ vs.} \text{ RHE} \quad (1)$$

$$CO_2 + 2H^+ + 2e^- \rightarrow HCOOH \quad E^0 = -0.12 \textit{ vs.} \text{ RHE} \quad (2)$$

$$CO_2 + 8H^+ + 8e^- \rightarrow CH_4 + 2H_2O \quad E^0 = +0.17 \textit{ vs.} \text{ RHE} \quad (3)$$

$$2CO_2 + 12H^+ + 12e^- \rightarrow C_2H_4 + 4H_2O \quad E^0 = +0.08 \textit{ vs.} \text{ RHE} \quad (4)$$

$$CO_2 + 6H^+ + 6e^- \rightarrow CH_3OH + H_2O \quad E^0 = +0.03 \textit{ vs.} \text{ RHE} \quad (5)$$

$$2CO_2 + 12H^+ + 12e^- \rightarrow C_2H_5OH + 3H_2O \quad E^0 = +0.09 \textit{ vs.} \text{ RHE} \quad (6)$$

The ECR reaction in aqueous electrolytes is normally divided into four stages: dissolution, activation, hydrogenation, dimerization and polymerization (Fig. 3). The first dissolution process is essential for the ECR in the aqueous electrolyte (Stage 1). In particular, a higher solubility of CO_2 usually implies a higher current density, which is vital for achieving industrially viable ECR rates. However, the dissolution and transport of CO_2 are limited due to their low solubility in water under ambient conditions (34 mM). This mass transport issue can be resolved by increasing the temperature or pressure to improve the solubility of CO_2 in electrolyte; using a gas diffusion flow cell to continually provide CO_2 saturated electrolyte, and modifying the electrode surface to optimize the hydrophobicity and aerophilicity of the electrode.

CO_2 is adsorbed and stabilized on the electrode surface after dissolution, resulting in two main products: *HCOO and *COOH (Stage 2 to Stage 3). The hydrogenation of *HCOO on the surface of the Group I catalysts, which have a weak binding force to *HCOO, results in HCOOH (Stage 3). *COOH is reduced to *CO (Stage 4), on the catalysts (Group II and Group III) with strong *COOH binding ability. Finally, Group II catalysts with weak binding to *CO produce CO. In contrast, Group III catalysts with strong binding with *CO prefer to undergo C–C coupling and generates C_2/C_{2+} products. In particular, the formation of C_2 and C_{2+} is called ''dimerization and polymerization'', respectively. Furthermore, the selectivity and adsorption capacity of intermediates is the most critical research field during the entire process. The Sabatier principle should be followed in the design of catalysts, which states that the interaction between the catalysts and intermediates should not be too strong or too weak.

2.2. Descriptors of ECR catalytic activity

The market price determines whether ECR can be widely accepted, which involves cost considerations. Apart from electrolytes, separators, and catalysts associated with electrolysis device; the cost of the entire ECR process includes CO_2 capture, electricity, product purification, transport, and storage. The descriptors directly related to the catalysts were the current density, Faraday efficiency (FE), energy efficiency (EE), and durability during the ECR process.

The target product's current density is not only an important indicator of reaction rate, but also an important factor in terms of electricity cost. This governs the size of the electrolyzer required for a given production rate. Generally, a large electrolyzer requires high current density to cover the capital cost. Sargent *et al.* found that the impact of the current density on the electricity cost gradually weakened once it exceeded 300 mA cm^{-2}.[32]

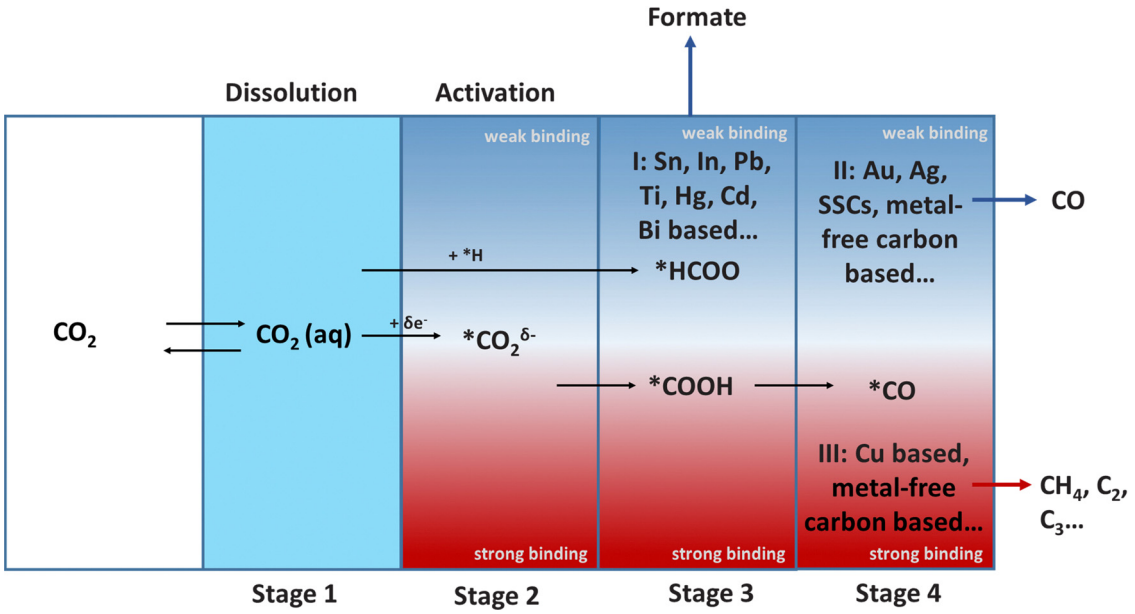

Fig. 3 The relationship between catalyst-intermediate binding energy and selectivity of products (* represents active site on catalysts surface).

Therefore, a high current density (>300 mA cm^{-2}) should be regarded as the basic standard to reduce the overall cost.

FE is another key indicator for describing the efficiency of charge (electron) transfer in systems that promotes targeted electrochemical reactions. A high FE toward a specific product could minimize the cost of product separation, which can help reduce current density and electricity cost. Thus, achieving a high FE, close to 100%, is always a worthwhile goal.

EE is the ratio of the output energy from the products of "what we gain" to the input energy from "what it cost" to produce them. Generally, the calculation of this parameter requires a comprehensive consideration of the FE and voltage efficiency of the product. Voltage efficiency reflects the part of the total input voltage that is actually used to drive the thermodynamic process, which is also related to the electricity cost. Therefore, a high EE is generally desired at low cost.

Durability is an extremely important parameter of ECR catalysts. After reaching the target current density, FE, and EE, robust stability effectively reduces the cost of maintenance and replacement. However, most current reports do not reach an ideal test time (more than 8000 h), which is important in the study of stability.

Generally, a suitable high current density (>300 mA cm^{-2}), high FE ($\sim$100%) and EE, and good stability (over 8000 h) are of great significance to promote the widespread application of ECR.

3. Single-atom catalysts

SACs, consisting of isolated metal atoms coordinated with non-metal atoms of supporting materials, are an emerging topic in the field of electrocatalysis.[34–39] SACs have received widespread attention because of their high activity and selectivity since Zhang *et al.* first proposed the concept in 2011.[40] Benefiting from their unique electronic structure and adjustable physico-chemical properties, SACs can maximize atomic utilization efficiency and possess an unsaturated coordination environment.[41,42] These unique features of SACs make them crucial for the oxygen reduction reaction,[35] HER,[36] ECR[34] oxygen evolution reaction,[37] and other catalytic processes.[38,39,43] However, the high surface energy of SACs facilitates their aggregation.[44] As a result, the choice of substrate is vital for the design of SACs. In particular, three families of supporting materials, carbon-based, oxide-based, and other supporting materials, are usually used for SACs applied in ECR.

3.1. Carbon-based SACs

Carbon-based materials are rarely used directly in ECR because of their high CO_2 adsorption energy barrier. However, their high specific surface area and strong interaction with metals are conducive to the formation of highly dispersed SACs.[45] Carbon materials also have many advantageous properties, such as high conductivity and good chemical stability, which make them ideal supporting substrates for SACs.

The bottom-up strategy is one of the most common methods for obtaining carbon-based SACs. In this method, metal ions are usually adsorbed on the surface of the carbon matrix; this is followed by drying and high/low-temperature thermal treatment to achieve firm anchoring.[46] Zhang *et al.* synthesized some SACs with different metal atoms (M-SACs, M = Ru, Fe, Ni, Cr, Cu, Zn, Pt, Mn, Co, *etc.*) (Fig. 4a–i) by employing a "ligand-mediated" synthetic strategy.[47] The strong covalent bond between the metal atoms and abundant defect sites on the surface of carbon black prevented the aggregation of metal species. Moreover, the use of carbon-supporting substrates circumvented the instability caused by high-temperature pyrolysis. Only graphite peaks were observed in the X-ray diffraction

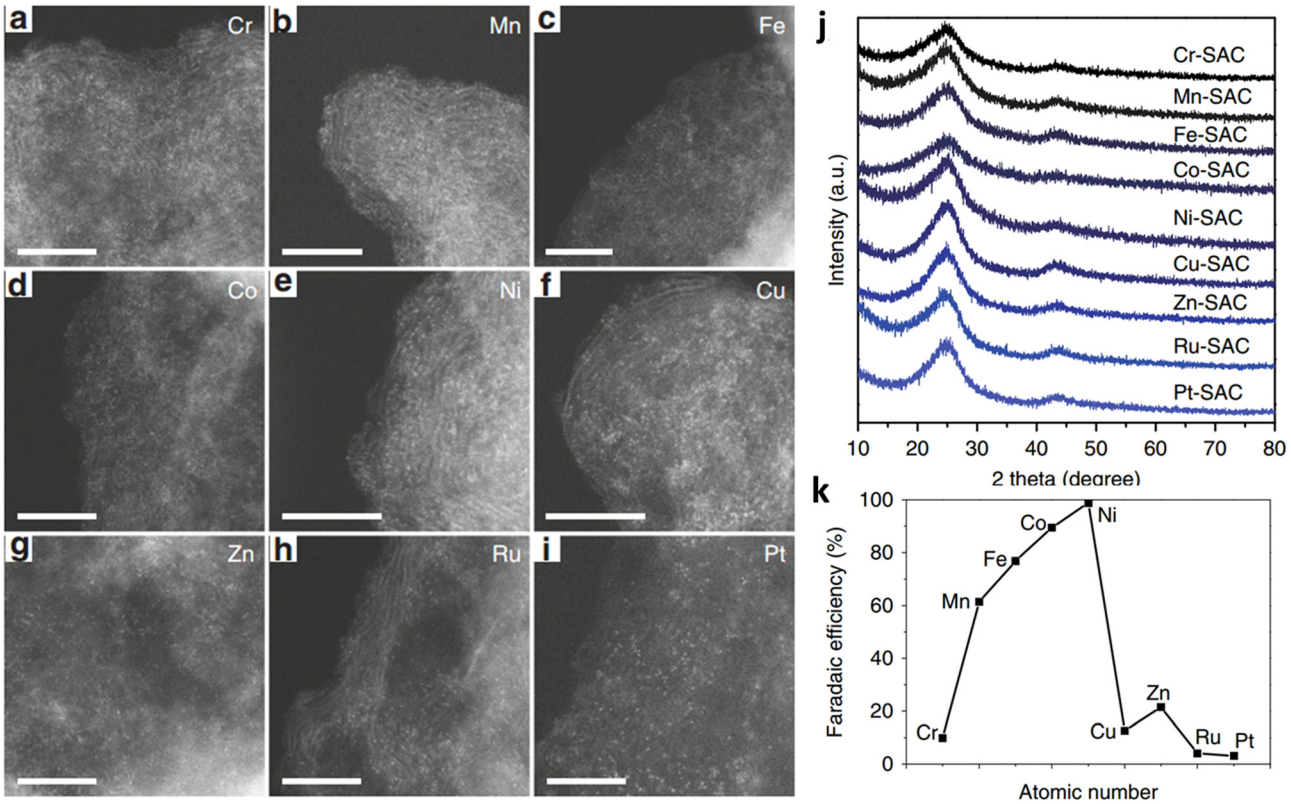

Fig. 4 (a–i) High-angle annular dark-field scanning transmission electron microscopy (HAADF-STEM) images for M-SACs. Scale bar: 5 nm. (j) XRD patterns for the M-SACs. (k) FE_{CO} for M-SACs at −1.2 V. Reproduced with permission.[47] Copyright (2019) Springer Nature.

(XRD) patterns of these M-SACs, indicating that the formation of metal nanoclusters could be prevented (Fig. 4j). Different M-SACs were measured at −1.2 V to compare the effect of different central metals on the ECR performance. A "volcano curve" is displayed in Fig. 4k, showing that the appropriate interaction between intermediates and Ni atoms makes Ni-SACs the most suitable candidate for ECR compared with other as-prepared M-SACs.

Efforts have been devoted to heteroatom doping (such as N, O, and S) in the carbon lattice to improve the catalytic performance.[48] Furthermore, the N dopant could be incorporated into carbon *via* pyrolysis of N-containing compounds (such as dicyandiamide,[47] melamine[49] and urea[50]) with carbon matrix (such as graphene,[51] carbon black,[50] and graphdiyne[52]), and products with different architectures (such as nanotubes,[53] nanosphere,[54] and nanosheets[53]) can be obtained. The introduction of N can effectively stabilize single-atomic centres for N-doped carbon-based SACs.[55,56] For example, Xie *et al.* enabled the activation and protonation of ECR through anchoring $Sn^{\delta+}$ atoms on N-doped graphene.[57] Furthermore, they performed *in situ* Fourier transform infrared (FT-IR) spectroscopy coupled with computational analysis and found that the N dopant could enhance the rate-determining HCOOH desorption step by decreasing the Gibbs free energy and elongating the bond length of Sn-$HCOO^-$ (Fig. 5a and b). Their experimental results agreed with the theoretical predictions. The as-prepared catalysts exhibited an onset overpotential below 60 mV and robust stability of more than 200 h (Fig. 5c), whereas their turnover frequency (TOF) was up to 11 930 h^{-1} (Fig. 5d).

Li *et al.* found that the metal-N site could serve as the active center.[54] They computationally showed that the as-prepared $Co–N_5$ is the rate-determining center for the transformation from $*CO_2$ to *COOH (Fig. 6a and b), which is a crucial process for CO desorption. The obtained CoN_5 coordinated on hollow N-doped porous carbon spheres ($Co–N_5$/HNPCSs) achieved a satisfactory FE_{CO} of approximately 90% (Fig. 6c and d).

Although N can contribute to ECR through pyrrolic N, pyridinic N or graphitic N. In general, the dominant contribution is derived from metals sites.[58,59] Strasser *et al.* found that once with the participation of metals, CO is further reduced to methanol and/or methane, indicating that the metal centers are dominant for the further reduction of intermediates during ECR by conducting controlled tests with or without metal (Fe or Mn) centers.[60]

Unsaturated coordination is also an important ECR performance improvement strategy for carbon-supported SSCs.[61,62] The bonding of common transition metal-N-doped carbon SACs to the reaction intermediates during the ECR process is relatively weak owing to the saturated coordination environment. Therefore, properly adjusting the coordination number to form an unsaturated coordination state helps improve the adsorption capacity of intermediates. Feng *et al.* proposed novel $Cu–N_2$ SACs on an ultrathin graphene matrix with unoccupied 3d orbitals of the central metal.[63] A reduction in the N

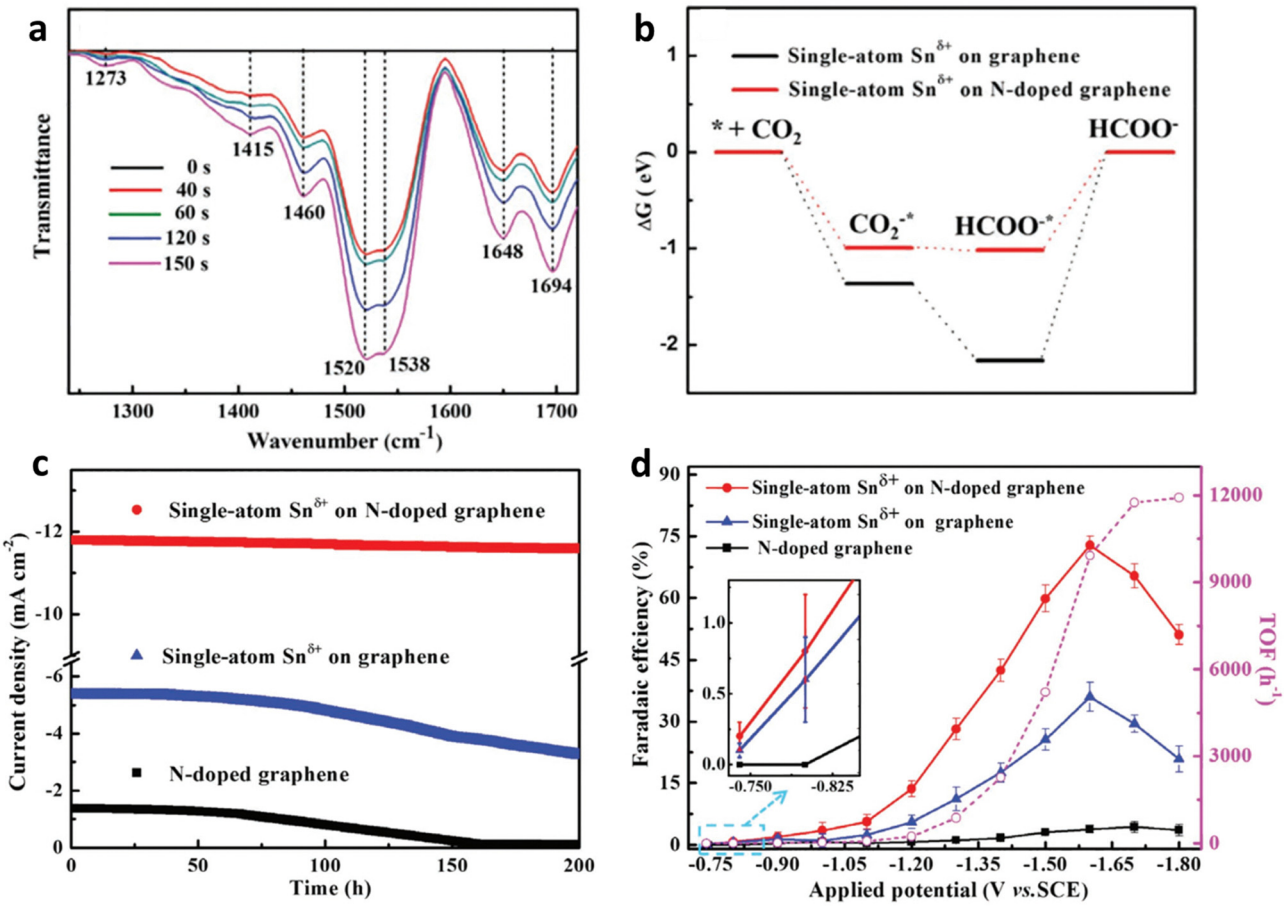

Fig. 5 (a) *In situ* FT-IR spectra of Sn-SACs. (b) Free energy diagrams. (c) Chronoamperometry tests at −1.6 V *vs.* SCE. (d) FE_{HCOOH} and TOF of the Sn-SACs. Reproduced with permission.[57] Copyright (2019) Wiley-VCH.

coordination number shortens the Cu–N bond length. Meanwhile, electron transfer from Cu–N_2 to *CO_2 is accelerated, thus promoting the hydrogenation of *CO_2 as well as the Zn–CO_2 battery performance.

Defect engineering also functions as an effective route to avoid the migration of isolated metal atoms and optimize the ECR process of carbon-based SACs.[53,61] Particularly, defects not only change the coordination environment but also modify the surrounding electronic structure, thereby forming unsaturated coordination sites or vacancies. These as-obtained coordination sites or vacancies are effective for anchoring metal atoms. In addition, carbon defects can be engineered to anchor metal atoms through electron transfer between carbon and metal atoms for carbon-based materials. These carbon defects usually result in a negative charge on the surface of the carbon material, which is helpful for the uniform adsorption of metal cations.[64,65] Furthermore, Wang *et al.* designed graphene oxide with high-density defects, which made the surface full of negative charges and helped to uniformly anchor a monolayer of Ni cations (Fig. 7a–c).[66] The density of single atom active sites could be increased to achieve high catalytic activity: a nearly 95% CO selectivity at 550 mV over-potential with the assistance of carbon defects (Fig. 7d and e). Furthermore, they found that by anchoring other transition metal (TM) single atoms (Co, Mn, *etc.*) into layered graphene vacancies (M-NG), the HER kinetics could be effectively suppressed, and suitable CO binding could be realized.

Through the design of carbon defects, the coordination number of metals can be regulated, thereby achieving the goal of anchoring more metals species with different characteristics.[63,67] Shui *et al.* first anchored the rare-earth metal atoms Y and Sc in large carbon defects (M/NC) by adjusting the coordination anion.[67] Furthermore, six M–N/M–C coordination bonds are required for anchoring each metal atom because of the large radii of Y and Sc (Fig. 8). Therefore, the catalyst exhibited a different coordination structure from that of MN_4, and it exhibited excellent performance in the nitrogen reduction reaction (NRR) and ECR.

MOF-derived SACs are another type of carbon-based SACs. Recently, MOFs have already received extensive attention due to their adjustable structure, size, and tunable active sites.[68–70] Furthermore, they inherit advantages from MOFs included rich three-dimensional (3D) channels and large surface areas, which are beneficial for electrolyte wettability and acceleration of mass diffusion. In addition, a favourable electronic environment of the active metal sites can be obtained in MOF-derived SACs owing to the coordination of various heteroatoms from

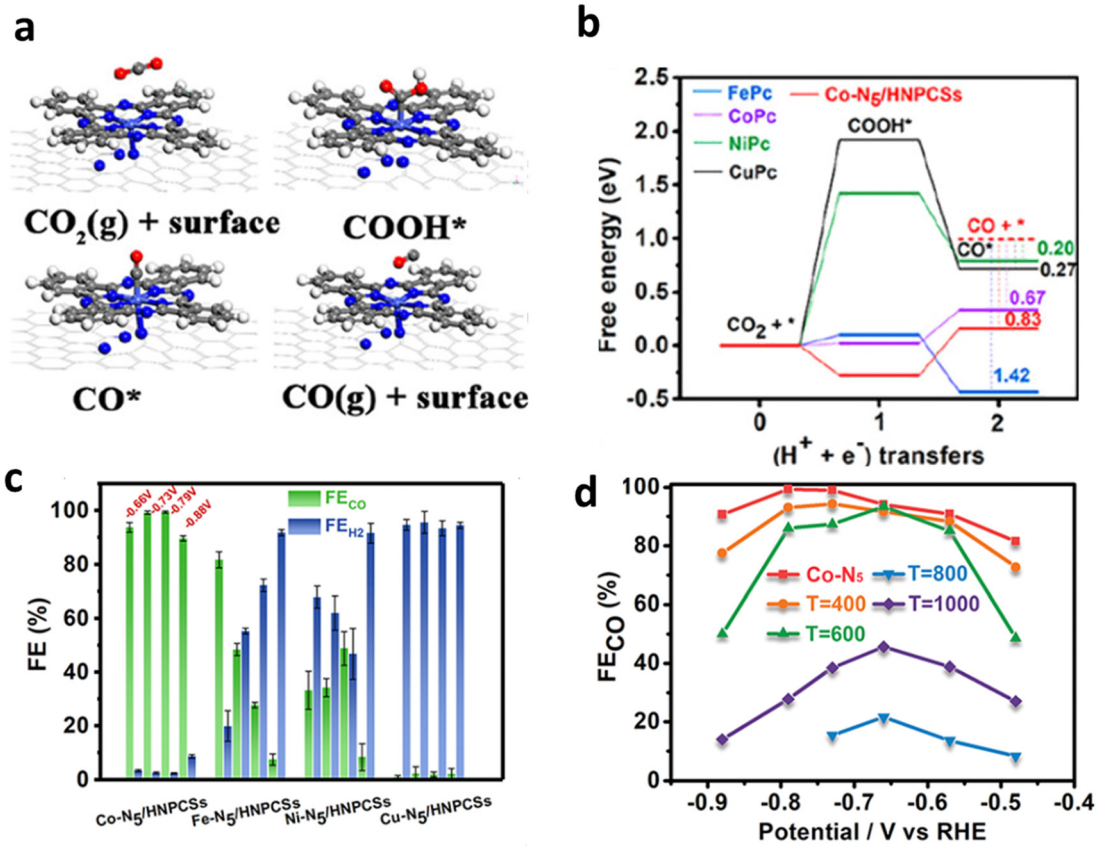

Fig. 6 (a) Schematic diagram of ECR reaction process on M–N_5/HNPCSs. (b) Calculated free energy. (c) FE of M–N_5/HNPCSs. (d) FE_{CO} of Co–N_5/HNPCSs-*T* (*T* = 400, 600, 800, and 1000 °C). Reproduced with permission.[54] Copyright (2018) American Chemical Society.

ligands, which is beneficial for ECR performance. The most common synthetic strategy for this type of material is using a zinc-based zeolitic imidazolate framework (ZIF-8) with rich N atoms as the supporting material. After one-step pyrolysis, Zn^{2+} is reduced to Zn and evaporated owing to its low boiling point, leaving abundant free N atoms to stabilize other high-boiling-point metals, such as Fe,[71] Co,[72] Ni,[73] Mn,[71] and Cu.[74]

There are two common strategies for the synthesis of SACs from ZIF-8. The first method involves directly mixing zinc salt with other metal sources and ligands in a system followed by calcination at a high temperature to obtain SACs.[75,76] The second method is to use the as-obtained ZIF-8 as a sacrificial template to mix with other metal species and form a uniform composite by ball milling,[77] electrospinning,[74] or other treatment,[78] and removing the Zn species through high-temperature pyrolysis. Furthermore, Jaouen *et al.* designed an atomically dispersed metal bonded to N atoms (metal-N_x) with a similar coordination environment by ball milling and pyrolysis of ZIF-8 and M^{2+} acetate (Fig. 9a).[77] As shown in Fig. 9b, a volcano trend was observed between the different metal centers and their activities toward CO formation. Operando X-ray absorption near-edge structure spectroscopy (XANES) and density functional theory (DFT) were performed to monitor the evolution of the active sites during ECR. The valence states of Co and Mn remained unchanged during ECR. However, Fe, Ni, and Cu were partially or completely reduced (Fig. 9c). The DFT results indicated that $M^{2+}N_4$–H_2O played the most important role in Fe- and Co-based catalysts, whereas $Ni^{1+}N_4$ was considered to be the intrinsic active sites in Ni samples at 0.5–0.6 V (Fig. 9d).

3.2. Oxide-based SACs

In addition to carbon-based and MOF-derived SACs, metal oxides (*i.e.* CuO,[79] FeO_x,[80] ZnO,[81] TiO_2,[82] and Al_2O_3[83] *etc.*..) can also serve as supports to anchor metal atoms. For instance, the strong adsorption ability of CeO_2 makes it a suitable substrate for the loading of different metal atoms. The CeO_2 based SACs have been widely used in CO oxidation,[84] hydrogenation,[85] and ECR.[86,87] Bao *et al.* prepared Au- and Ag-doped CeO_2 with promoted ECR performance.[86] Zheng *et al.* reported the use of Cu-doped CeO_2 SACs for ECR based on the strong interactions between CeO_2 and Cu.[87] The introduction of Cu favored the formation of single-atom Cu with a high oxygen vacancy (V_o) number of three. In particular, this structure would exhibit a bent structure with more efficient activation toward $CO_2^{\bullet-}$ when compared to single-atom Cu with V_o numbers of one and two (When the V_o is higher than three, the structure will be destabilized) (Fig. 10). Additionally, the FE_{CH4} of as-prepared Cu-doped CeO_2 SACs reaches ~58% at −1.8 V in the H-cells.

3.3. Other SACs

Metal nitrides and carbides are also important substrates for single-metal atom anchoring.[88–90] The p-orbits of N/C can perturb the d-orbits of the transition metal atoms, resulting

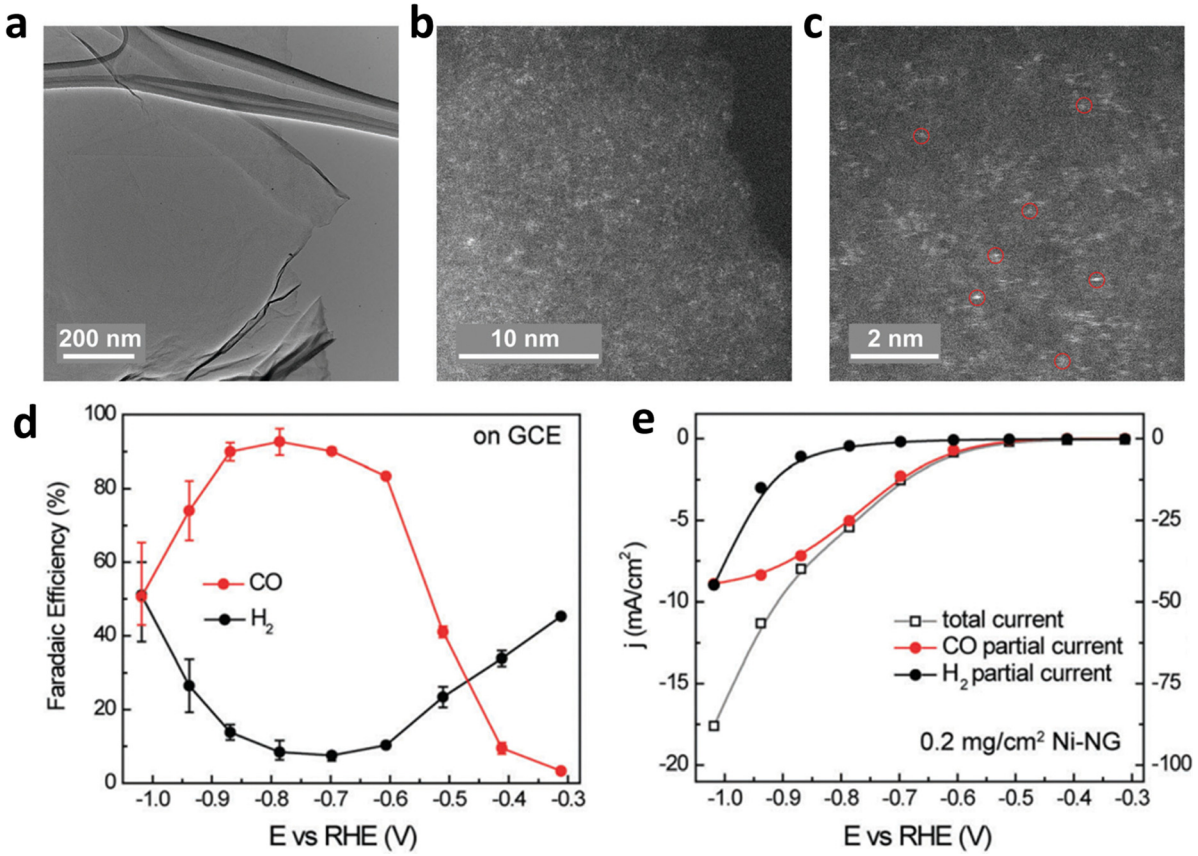

Fig. 7 (a–c) Structure characterization of Ni–NG; (d) FE_{H_2} and FE_{CO} and (e) the linear sweep voltammetry (LSV) curves of Ni–NG. Reproduced with permission.[66] Copyright (2018) Royal Society of Chemistry.

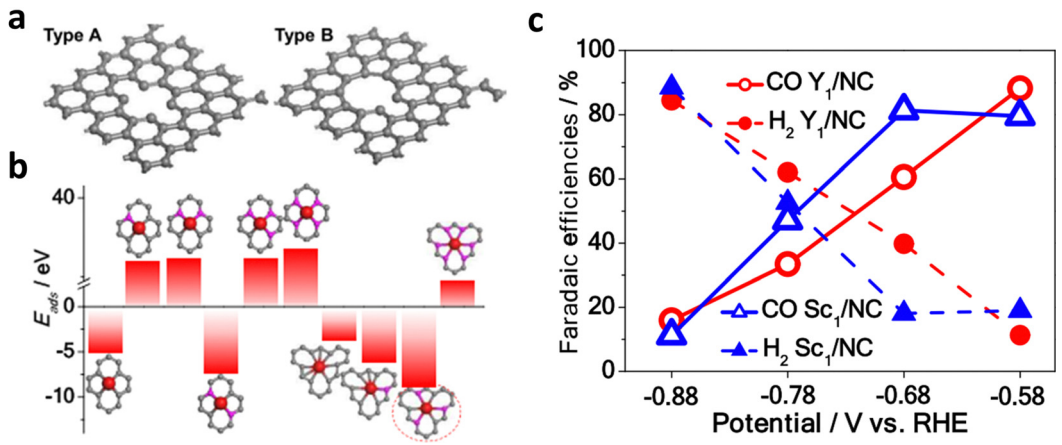

Fig. 8 (a) Structural diagram of type A and type B substrates with small-size and large-size carbon defects, respectively. (b) Calculated adsorption energies of different active sites of Y/NC. (c) FE_{CO} and FE_{H_2} of Y/NC and Sc/NC from −0.58 V to −0.88 V. Reproduced with permission.[67] Copyright (2020) American Chemical Society.

in interesting regulation of the metal active sites owing to the hybridization of the orbits. Furthermore, their good electrical conductivity and physicochemical stability make them suitable supports for SACs. Jung *et al.* recently used theoretical calculations to study the catalytic properties of TiN, TiC, and single atoms loaded onto them in the ECR.[88] TiC only needs −0.47 V limiting potential to drive the occurrence of ECR as a substrate, while TiN is easily poisoned by oxygen-containing species because of its strong affinity to O (Fig. 11a and b). In particular, the *CO binding site and strength of the catalyst changed

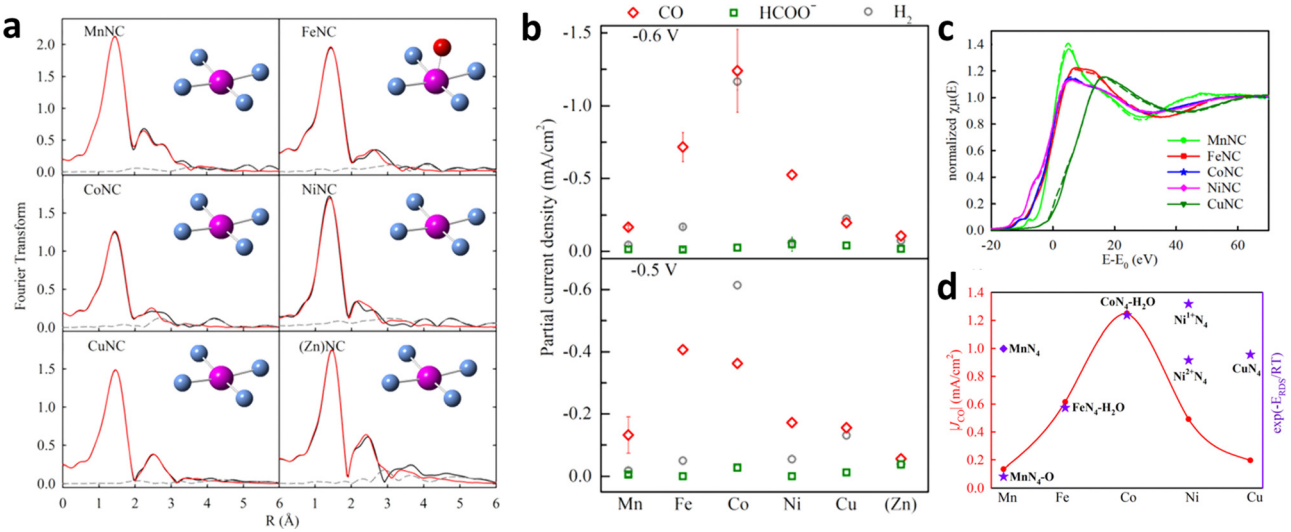

Fig. 9 (a) K-edge EXAFS spectra of MNC. (b) Partial current densities (J_p) over the MNC catalysts for different products. (c) K-edge XANES spectra of MNC before (solid curve) and after (dashed curve) the chronoamperometry test at different potentials. (d) CO j_p at −0.6 V for other MNC and computational trendency (U = −0.6 V). Reproduced with permission.[77] Copyright (2019) American Chemical Society.

owing to the interaction between the metal and the support. Compared with bare TiC and Ir(111), Ir on the TiC support lacks a Sigma-type interaction between Ir and *CO, thus reducing the limiting potential (Fig. 11c–f).

MoS_2 is a two-dimensional (2D) layered material with many application scenarios.[91,92] Various single atoms anchored on MoS_2 also have good application prospects in ECR.[93,94] It should be noted that MoS_2 could also be employed directly for ECR, and its edges are more active than its inert surface.[93,95] Activating the surface of MoS_2 by anchoring various single-atomic metals could also be a good choice for enhancing the ECR performance because the stability of edges is usually limited by the edge structure and reaction conditions.[96,97] By changing the mass loading of Pt, Zeng *et al.* prepared Pt monomers on MoS_2 with different percentages of isolated Pt and neighboring Pt (Fig. 12a–c).[96] These two kinds of monomer Pt with different coordination environments showed completely different selectivities towards ECR. Pt single atoms prefer the conversion of CO_2 into CH_3OH instead of HCOOH. However, CO_2 is easily hydrogenated into HCOOH and CH_3OH for neighboring Pt atoms (Fig. 12d and e).

Although SACs have a number of advantages, they also face some challenges: (1) materials that can be applied as precursors are still limited. As for MOF-derived SACs, the common MOFs used are limited to ZIF-8, UiO-66-NH_2, MIL-101-NH_2, and ZIF-67, and the supported single metal atoms are restricted

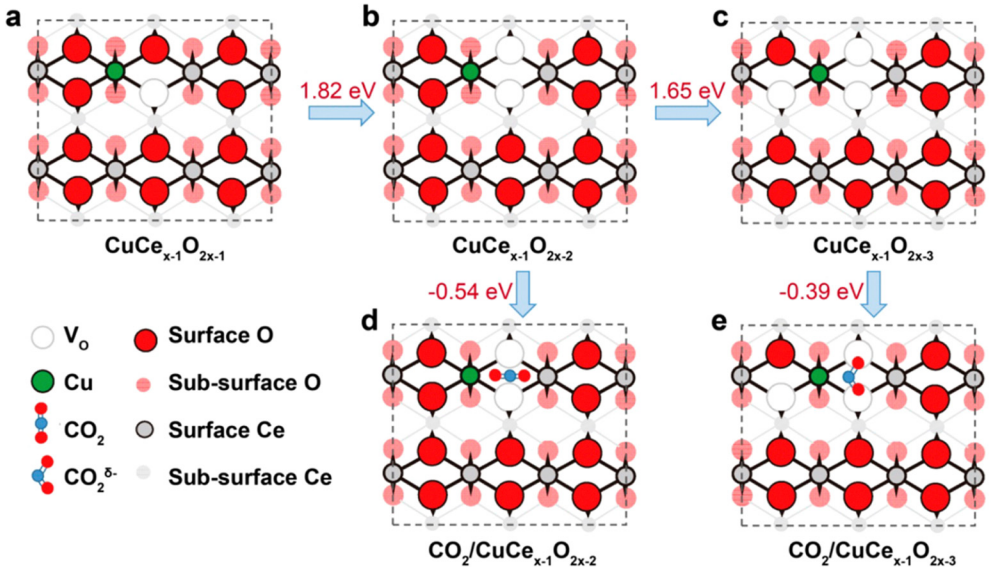

Fig. 10 (a–c) Structural diagrams of Cu doped CeO_2, with 1–3 V_o. (d and e) CO_2 adsorption and activation structural diagrams of these structure. Reproduced with permission.[87] Copyright (2018) American Chemical Society.

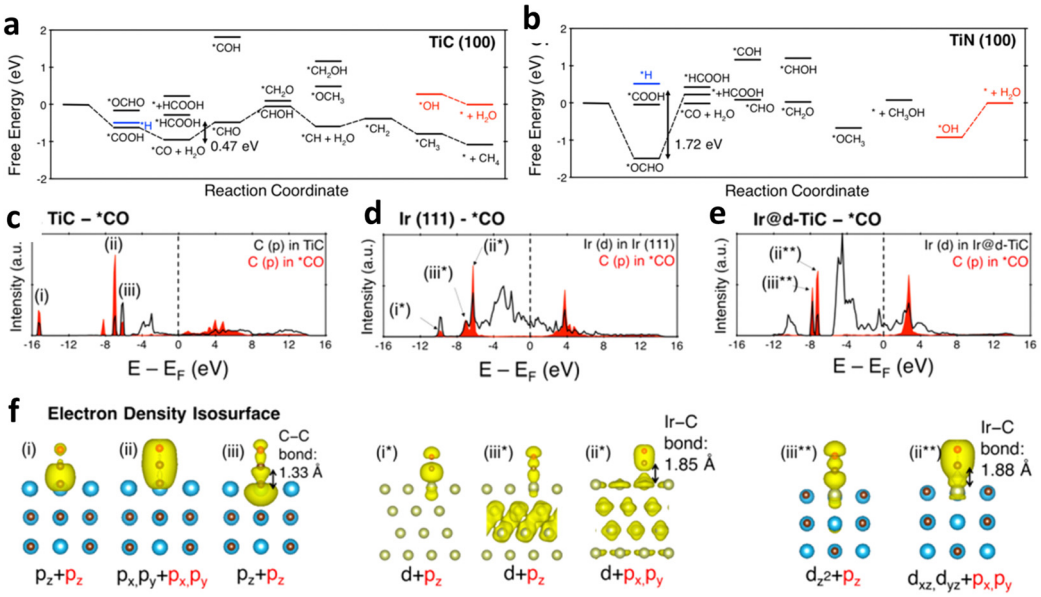

Fig. 11 Free-energy profiles for ECR on (a) TiC and (b) TiN. Density of states of (c) TiC, (d) Ir, and (e) Ir@d-TiC interacting with *CO. (f) The electron density isosurfaces at noted panels of (c–e). Reproduced with permission.[88] Copyright (2017) American Chemical Society.

to Fe, Co, Ni, Cu, Bi, *etc.* Thus, efforts should be dedicated to exploring additional supporting substrates, precursors, and metal species. (2) High-temperature treatment is typically required to obtain SACs. The metal loading is limited to avoid the

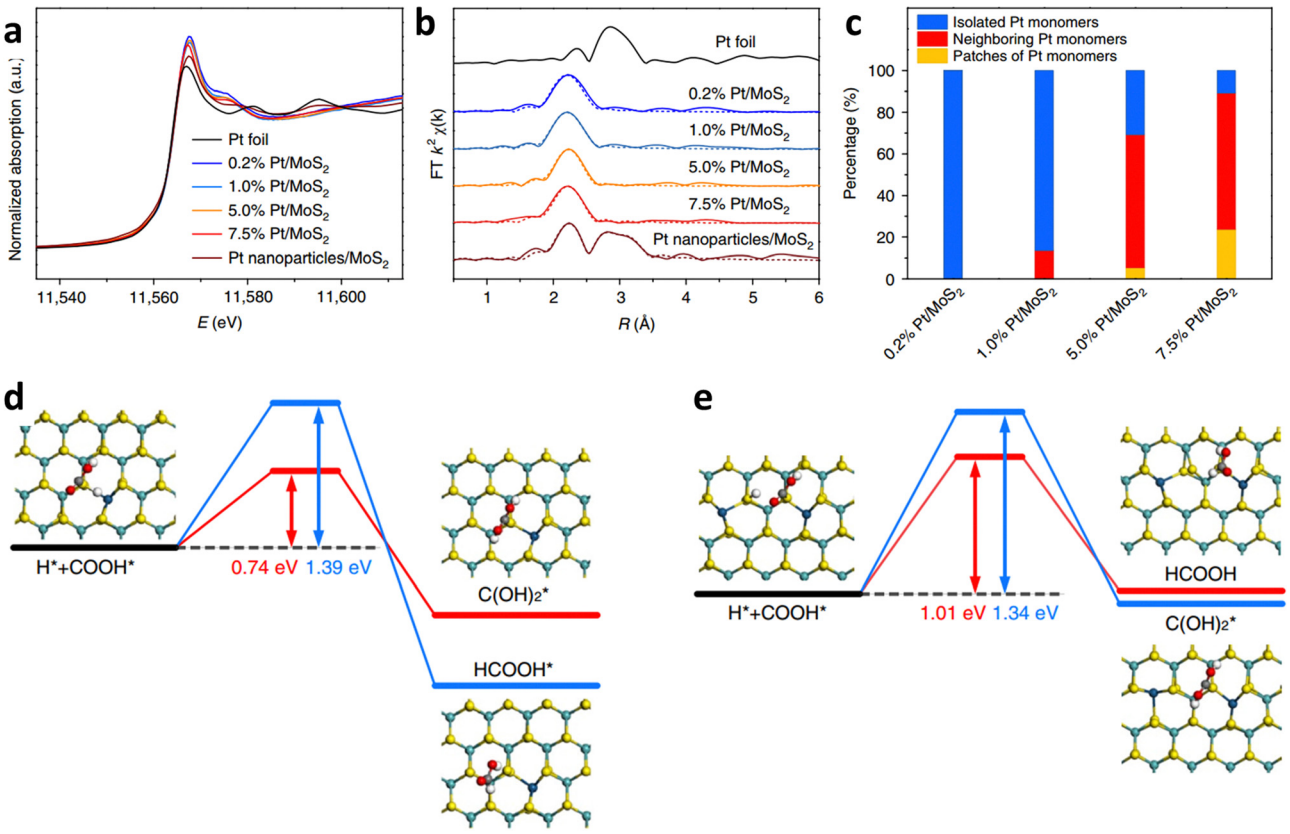

Fig. 12 (a) Pt K-edge XANES spectra and corresponding R space (b) for different Pt/MoS_2. (c) Bar graph showing the different Pt monomer contents of Pt/MoS_2 samples based on HAADF-STEM results. (d and e) Steps for the hydrogenation process of Pt_1/MoS_2 and Pt_{2iii}/MoS_2. Reproduced with permission.[96] Copyright (2018) Springe Nature.

agglomeration of metal atoms in a high-temperature environment. Therefore, the development of novel large-scale tactics to prepare SACs with high single-metal loadings is very important. (3) Morphology regulation is an important method to improve ECR activity. However, the morphologies of SACs synthesized are usually irregularly shaped particles after high temperatures treament. The design of better-defined morphologies remains a challenge. (4) Their structural characterization techniques are often limited to particular methods such as X-ray absorption spectroscopy and spherical aberration-electron microscopy because of the low loading of single atoms and their special structural properties. Therefore, it is important to develop new characterization methods for SACs.

4. Homogeneous molecular catalysts

HMCs are another family of emerging catalysts, which show great potential for high selectivity and activity in the ECR because their ligands can be finely tuned easily.[98,99] This kind of catalyst has a well-defined structure and active sites that allows for an in-depth study of the structural model and reaction mechanism of multi-proton–electron coupling in the ECR process, to establish a more intuitive structure–property mechanism–performance relationship. HMCs commonly used in ECR can be divided into phthalocyanine, porphyrin, dipyridine, and their derivatives (Fig. 13a).[100] Different types of HMCs in ECR products usually depend on the metal active site. As shown in Fig. 13b, for Mn-, Fe-, Co-, Ni-, Zn-, and Re-based HMCs, CO is the main product, whereas for Ir- and In-based HMCs are more inclined to produce formic acid. For Cu-, Ru-, and Rh-based HMCs, hydrocarbons occupy a large proportion of the products.[100–105] However, they all face the challenges of aggregation and demetallation owing to the solubility and side reactions in the reaction process regardless of the metal-based HMCs.[106,107]

Modifying the surface of HMCs is an important strategy to alleviate the aggregation issue.[108,109] HMCs are more prone to agglomeration in aqueous solutions than in organic solutions because of their special synthesis environment. This reunion further blocks or severely hinders the mass transfer process around the active sites, thereby reducing the stability decay and current density. This problem can be addressed by introducing hydrophilic groups. Furthermore, Officer *et al.* effectively improved the solubility of the catalyst by introducing alkoxy groups to CoPc (CoPc-A) (Fig. 14a), which prevented its agglomeration. However, the inherent activity of the catalyst was greatly enhanced (TOF of ~5 s^{-1} at an overpotential of 0.480 V). In addition, the as-prepared catalysts showed stable CO conversion for more than 30 h (Fig. 14b–d).[108]

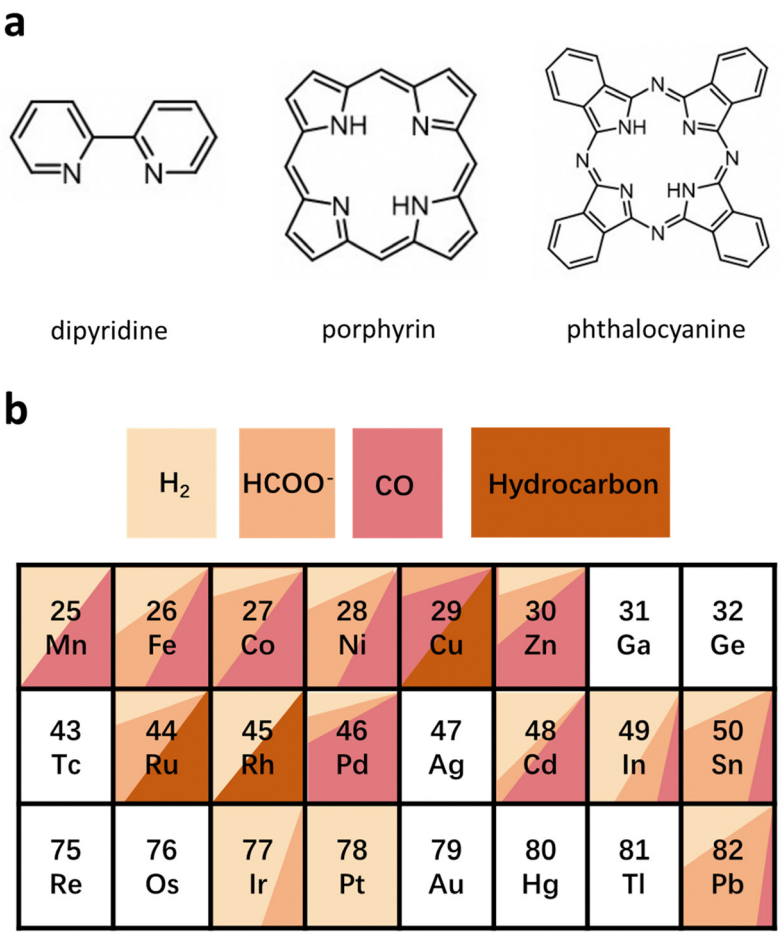

Fig. 13 (a) Common central ligand units for HMCs. (b) Product distribution of ECR on common HMCs.

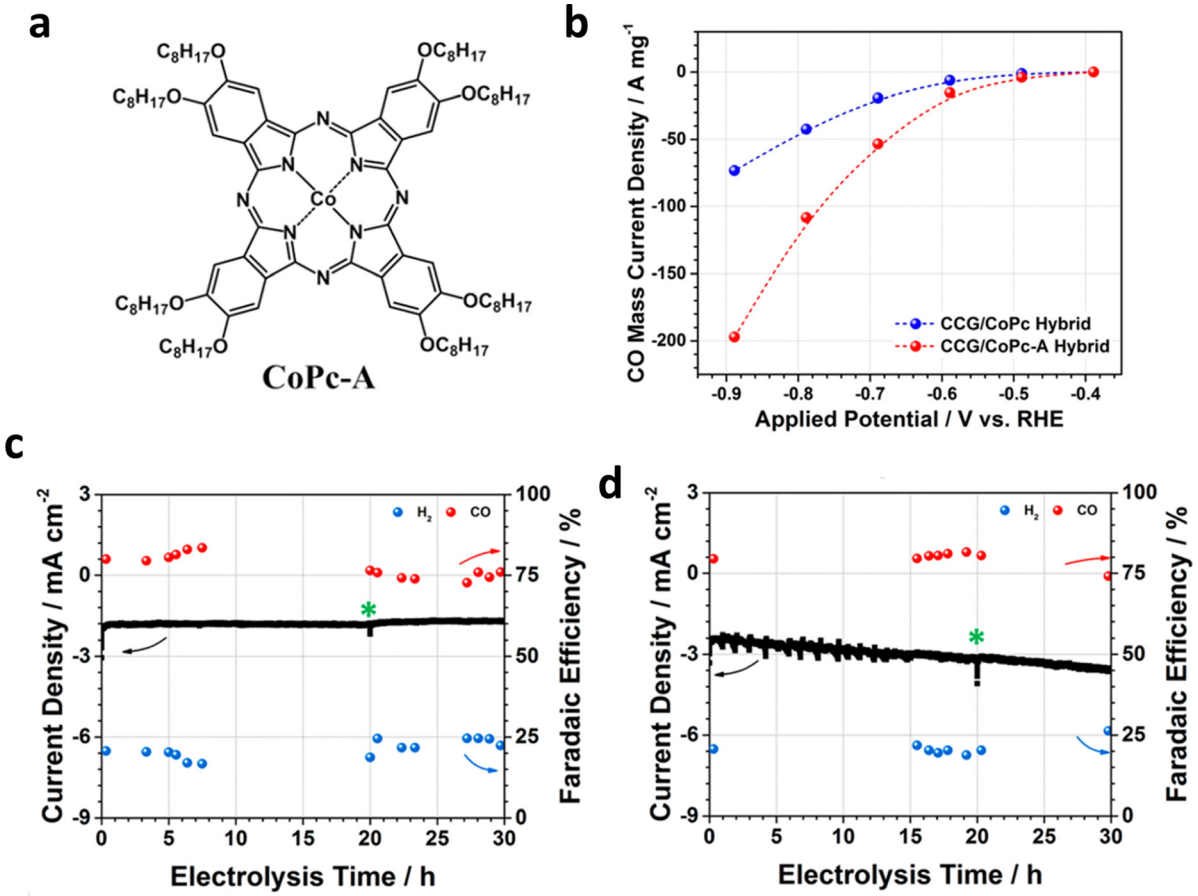

Fig. 14 (a) Structural diagram of CoPc-A. (b) Total current density (J_t) of chemically converted graphene/CoPc-A (CCG/CoPc-A) and CCG/CoPc hybrids. Stability test of (c) CCG/CoPc and (d) CCG/CoPc-A at same potential (−0.69 V). Reproduced with permission.[108] Copyright (2019) American Chemical Society.

Using a water-soluble HMC-modified electrode also alleviates the aggregation of the catalysts. Wang *et al.* effectively suppressed HER in the aqueous solution by depositing water-soluble 1,10-phenanthroline–Cu (phen–Cu) molecular complexes on a mesoporous graphene electrode.[109] *In situ* attenuated total reflection infrared (ATR-IR) study revealed that Cu molecules would heterogenize near the electrode during the test, resulting in an increase in electron density under catalytic conditions (Fig. 15a and b). Furthermore, they found that the phen–Cu surface structure of the graphene electrode affected charge distribution during the ECR process based on the infrared signal. The change in the applied potential confirms that the external electric field is crucial for the reversible heterogenization of Cu molecules (Fig. 15c). In addition, more electrons would aggregate on the ligands, owning to the reduction of the potential, thus leading to a blue shift in the IR spectra (Fig. 15d). Furthermore, the mesostructure of the graphene matrix limits mass transfer from the bulk solution to the electrode, thus suppressing the HER and greatly improving the selectivity of ECR. The modified catalysts exhibited enhanced TOF (45 s^{-1} at −1.0 V) and high FE_{CO} around 90% at −0.6 V. These results emphasize that the modification of the electrode surface with a suitable molecular catalyst can also achieve high ECR selectivity.

The reduction and demetallation of center metals are common side reactions of HMCs during the ECR process.[110–112] Actually, proper metal reduction could be helpful to the activation of ECR. Based on operational spectroscopy and electrochemical kinetics studies, Liu *et al.* found that Ni^+ produced by *in situ* reduction of Ni^{2+} in Ni(II) 2,9,16,23-tetra(amino) phthalocyanine (Ni–TAPc) is very active for ECR activation and can act as the intrinsic catalytic sites for ECR.[113] When the cathode potential was increased above 0.57 V under Ar atmosphere, a red-shift occurred for the Ni–N vibration in Ni–TAPc. Electrons were transferred to the Ni 3d orbital during the test, which led to the reduction of Ni^{2+} to Ni^+ (Fig. 16a). Once CO_2 was pumped into the system, the vibration of Ni–N will return to its pristine state (Fig. 16b), and no longer change with the changing cathode potential (from open circuit potential to 0.37 V). The quick oxidation of Ni^+ is believed to be more helpful than that of Ni^{2+} for the activation of CO_2 because it overlaps better with the C 2p* orbital in CO_2. Furthermore, the developed Ni SSCs showed high ECR activity with a FE_{CO} of 99% and TOF of 100179 h^{-1} (Fig. 16c and d).

However, the irreversible metal reduction or demetallation reaction can easily lead to the formation of large-size metal particles, which would lead to the decay of the catalytic activity. Wang *et al.* designed a controlled ECR experiment with three

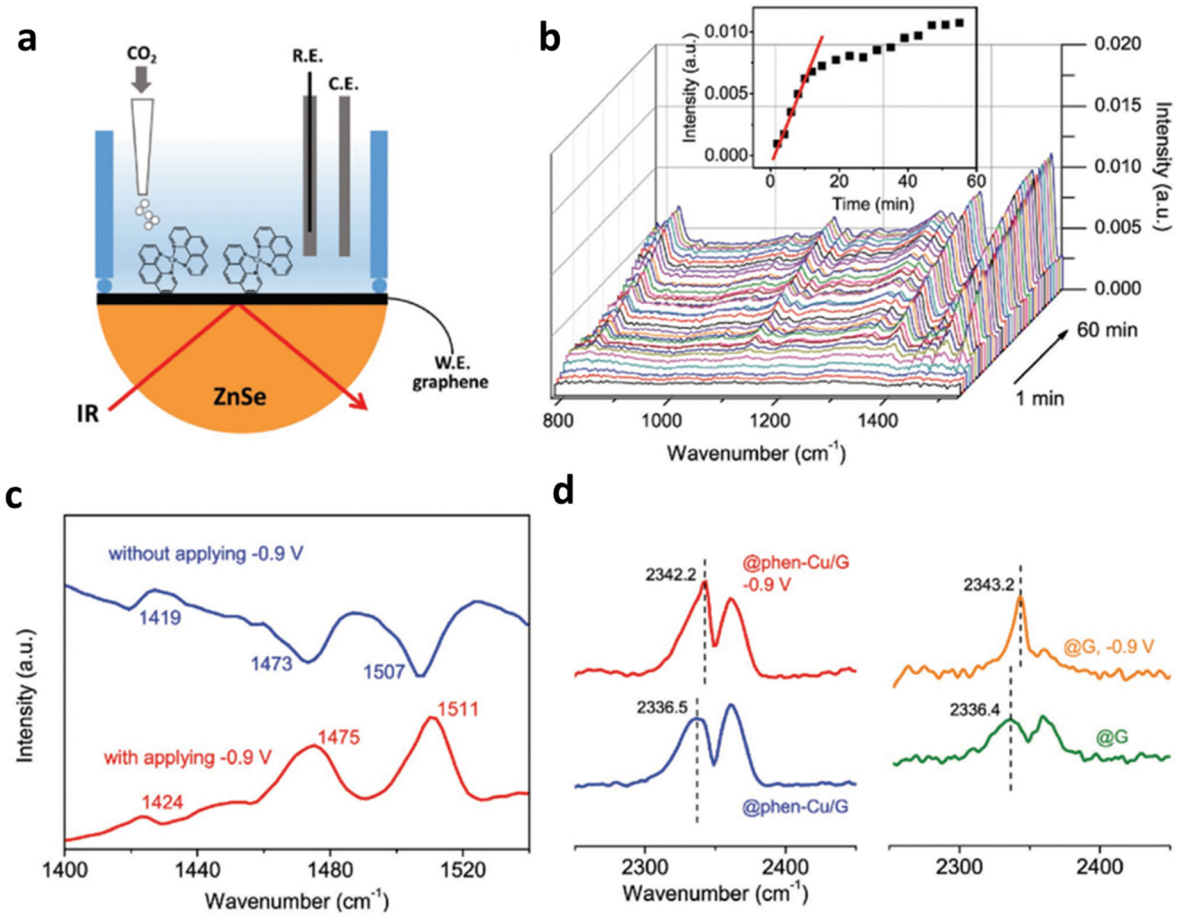

Fig. 15 (a and b) *In situ* Raman spectrum tests of Ni–TAPc on gold electrode under (a) Ar and (b) CO_2. Electrochemical performance: (c) FE_{CO} and J_t at different potentials acquired on a carbon cloth electrode in CO_2-saturated 0.5 M $KHCO_3$ solution. (d) TOF of Ni–CNT–CC (Ni–CNT represents Ni–TAPc anchored on carbon nanotubes) compared with other CO_2-to-CO catalysts. Reproduced with permission.[109] Copyright (2018) Wiley-VCH.

Cu complexes: CuPc, Cu-based HKUST-1, and $[Cu(cyclam)]Cl_2$ (Fig. 17a–c).[110] They found that the CuPc exhibited the highest activity and selectivity among all catalysts; its partial current density for methane and FE_{CH4} reached 13 mA cm^{-2} and 66% at −1.06 V, respectively (Fig. 17d and e). Additionally, the CuPc exhibited the highest activity and selectivity among all the catalysts. It showed high partial current density for methane (13 mA cm^{-2}) and FE_{CH4} (~70%), respectively (Fig. 17d and e). Operando XANES and extended X-ray absorption fine structures (EXAFS) were applied to probe the reconstruction of the local coordination environment during the ECR. However, during the ECR process, the CuPc molecules underwent reconstruction and produce nearly 2 nm metallic Cu clusters. Additionally, the Cu nanocluster quickly reverted to the pristine structure after applying the negative electrode potential (at 0.64 V) (Fig. 17f–h). On the contrary, for $[Cu(cyclam)]Cl_2$ and HKUST-1, the complexes decomposed and agglomerated into larger Cu particles, which also explains their poor ECR activities. They applied DFT to examine the thermal kinetics of the reductive demetalization and recovery of the CuPc structure to better study the reconstruction process. The calculations show that the demetallization process has lower reduction potential than those of the other two catalysts. This indicates that CuPc has the most stable structure among all Cu-based catalysts. Thermodynamic calculations also revealed that the binding affinity of the metal ions of the copper complex with the ligands affects the threshold potential and reversibility of the reductive demetallization process, influencing the ECR performance further.

For HMCs, their ligands can be easily fine-tuned during the synthesis process, giving them greater controllability and advantages in performance and model establishment. Their good solubility in organic solvents and water also expands their application scenarios, though they still face many challenges: (1) the low loading capacity of HMCs makes them insensitive to traditional characterization methods. However, HMC must prioritize selectivity and stability. (2) The HMCs currently used in the ECR direction are limited to bipyridine, porphyrin, and phthalocyanine derivatives. Thus, the development of HMCs with novel ligands and product selectivity is critical. (3) The methods for HMC immobilization are currently limited (such as π–π interactions, physical confinement, and covalent bonding). Stability is another big challenge; the choice of immobilization needs to consider the problems of catalyst leaching, demetallation, aggregation, and steric hindrance of ligands. Furthermore,

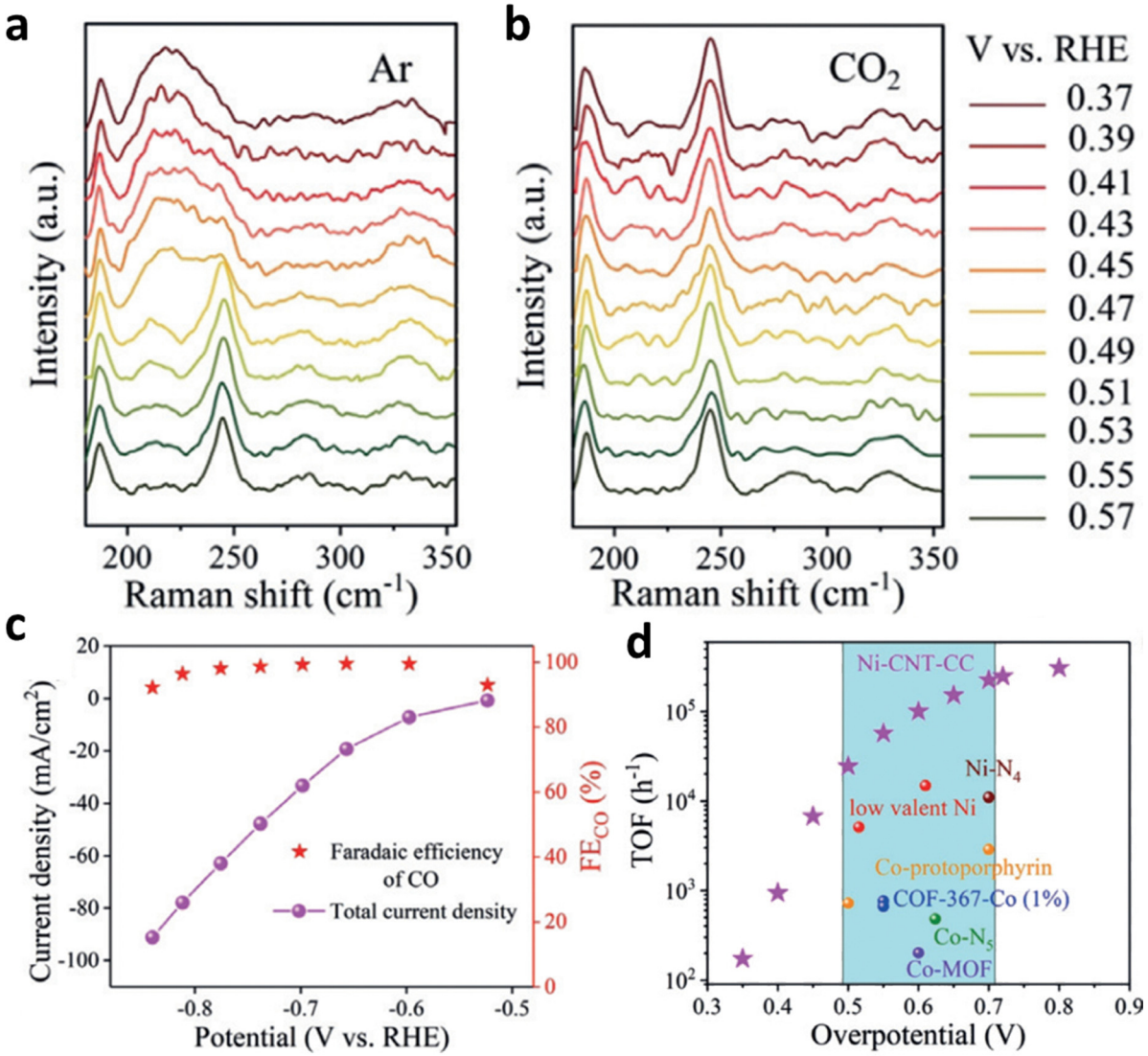

Fig. 16 (a and b) Raman spectra of Ni–TAPc collected on an Au electrode at various potentials under (a) Ar (1.0 atm) and (b) CO_2 (1.0 atm). Electrochemical performance: (c) FE_{CO} and J_t at different potentials acquired on a carbon cloth electrode in CO_2-saturated 0.5 M $KHCO_3$ solution. (d) The TOF of Ni–CNT–CC (Ni–CNT represents Ni–TAPc anchored on carbon nanotubes) compared with those of other CO_2-to-CO reduction catalysts. Reproduced with permission.[113] Copyright (2020) Wiley-VCH.

it will be necessary to further develop assembly technology and introduce more kinds of ligands into the skeleton to help improve the diversity and mechanism research of molecular catalysts in the future.

5. MOF-supported single-site catalysts

MOFs are emerging porous coordination polymers constructed from metal ions, clusters, and ligands. They have attracted considerable attention for broad applications owing to their large surface areas, well-defined metal nodes, and adjustable pore dimensions.[114,115] In addition, they also have attracted great interest in ECR because of their uniform and unique geometry and electronic structure.[116–119] In contrast to the MOFs that serve as the precursor for SACs in Section 3.1, the MOFs in this section act as supporting substrates for atomic metal sites. Particularly, apart from only being applied to avoid agglomeration and deactivation through the physical separation of individual catalyst molecules compared with other porous supports, MOFs can also be used for an in-depth study of the ECR mechanism by deeply exploring the relationship of structure–property relationship. The highly ordered arrangement of metal nodes and organic ligands with sub-nanometer-sized pores enables MOFs to disperse atomic-level metal sites altogether. Thus, in this section discusses the SSCs located in the metal nodes, ligands, and pores.

5.1. SSCs located in metal nodes

Anchoring a single atomic site on the metal nodes achieves a uniform distribution and avoids aggregation because of the

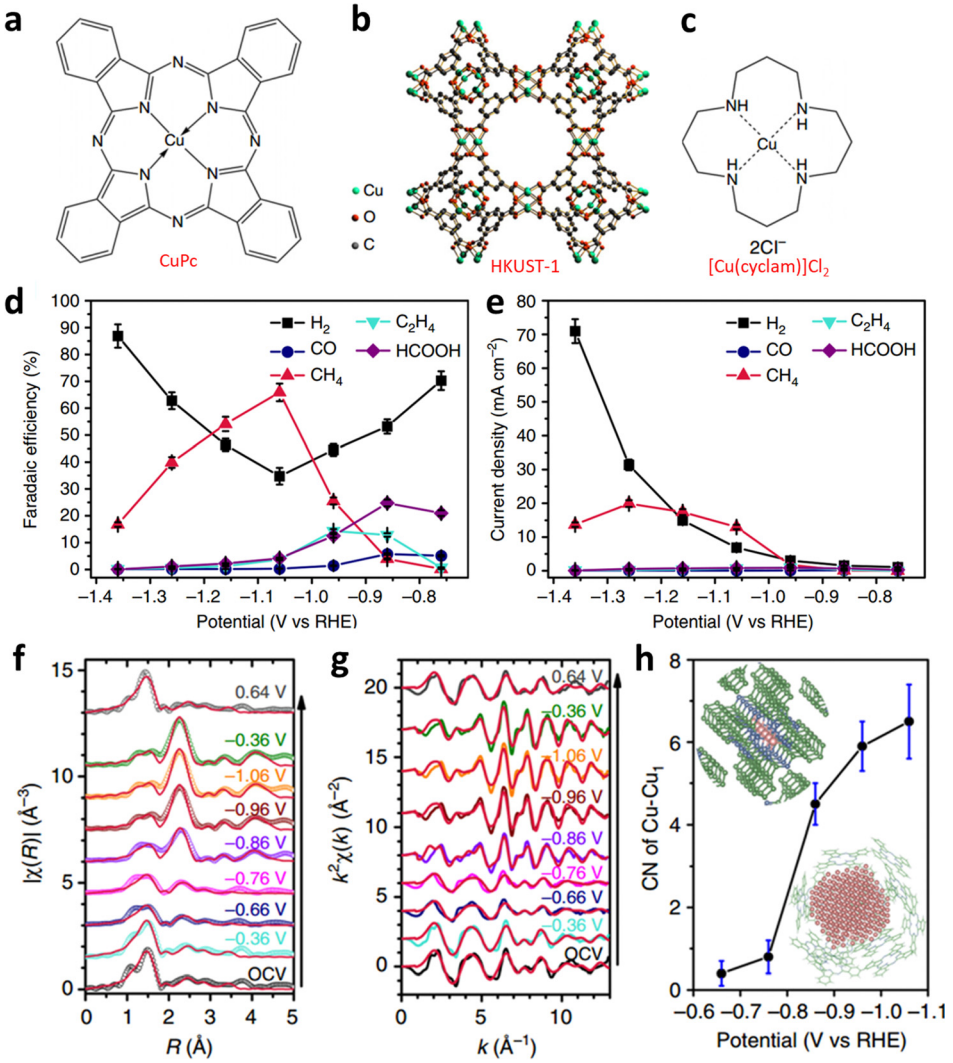

Fig. 17 Structural diagram of (a–c) three Cu complexes. (d) Potential-dependent FE and (e) j_p of products for ECR catalyzed by CuPc. Fitted (f) *R*-space and (g) *k*-space EXAFS spectra of CuPc. (h) First-shell Cu–Cu coordination numbers of CuPc from −1.5 to −0.65 V. Reproduced with permission.[110] Copyright (2018) Springer Nature.

uniform distribution of metal nodes in MOFs. Metal nodes are usually built by metal oxide clusters such as ZrO_{6-8} and $Zr_6O_4(\mu_3\text{-}OH)_4$, which act as binding sites on MOFs.[109,120] Their unsaturated coordination environment makes them ideal substrates for anchoring isolated metal atoms. Furthermore, Gu *et al.* prepared TCPP(Co)/Zr-BTB MOF nanosheets by constructing an interaction between the Zr_6 clusters of Zr-BTB MOF (BTB = one, three, 5-tris(4-carboxyphenyl)benzene) and carboxyl groups of Co porphyrin [TCPP(Co)] (Fig. 18a).[18] The obtained 2D structure could avoid the stacking of cobalt porphyrin and guarantee the full exposure of active sites to CO_2, which greatly optimized the ECR efficiency with a 77.2% FE_{CO} and a 7 mA cm^{-2} j_t (Fig. 18b and c). Moreover, they introduced different ligands to Zr_6 groups, *p*-(aminomethyl)benzoic acid (PABA), *p*-sulfobenzoic acid potassium (PSBA), and *p*-sulfamidobenzoic acid (PSABA), to create different microenvironments around TCPP(Co). After modification, the as-prepared TCPP(Co)/ZrBTB not only inherited the pristine structure, but also maintained the uniform nanosheet morphology. The HER has been inhibited, and the FE_{CO} of the PSABA-modified catalysts reached 85.1%, thus benefiting from the steric effect and tighter coverage of Zr_6 clusters derived from modifier molecules (Fig. 18d and e).

Using an external electric field to promote the coordination of molecules with single metal sites and MOFs is also an effective method to prepare SSCs located on MOF nodes. Furthermore, Joseph *et al.* realized the heterogeneous electrochemical conversion of carbon dioxide (~100% $FE_{(CO+H_2)}$) to fuel under high flux conditions, by electrophoretic deposition of a large number of Fe-porphyrin (Fe-TPP) based MOF-525 (Fe_MOF-525) on fluorine-doped tin oxide (FTO), (Fig. 19a).[22] Additionally, they achieved a high concentration of Fe-TPP adsorption, equivalent to approximately 900 layers of Fe-TPP adsorbed on the FTO surface by selecting appropriate MOFs (Fig. 19b). In addition to the introduction of Fe single-site molecular catalysts, the ECR selectivity of the original electrodes could be optimized. Moreover, the

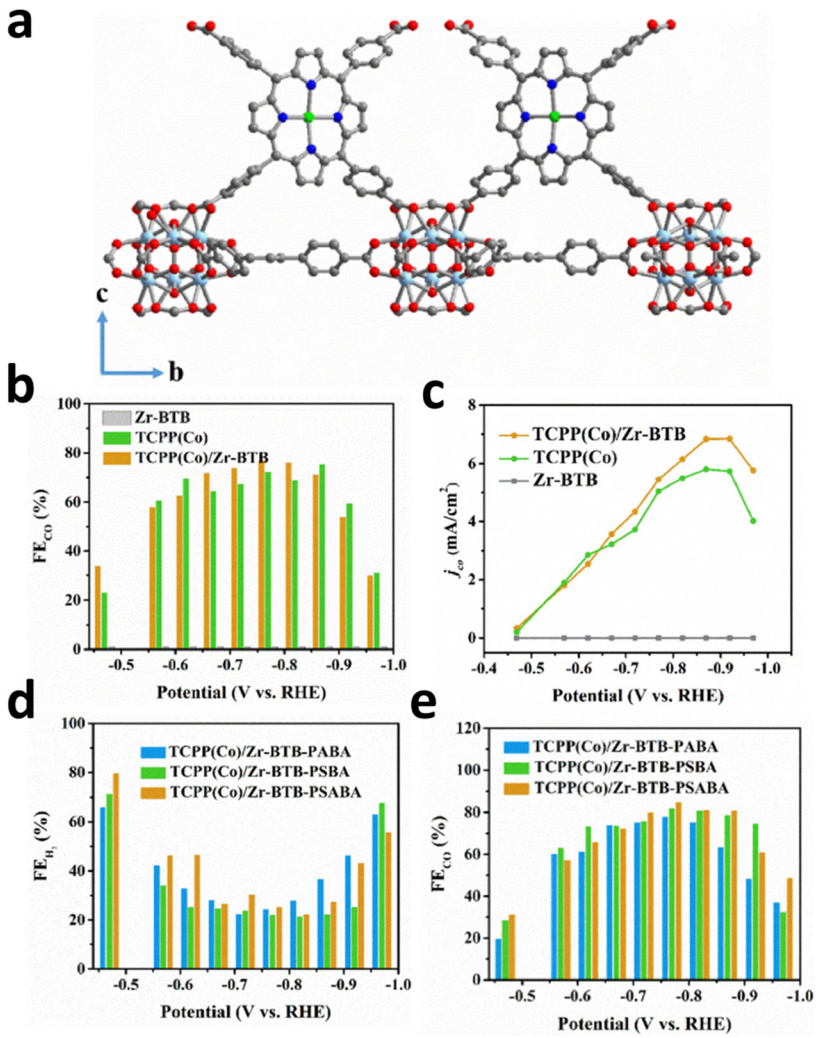

Fig. 18 (a) Schematic diagram of TCPP(Co)/Zr-BTB. (b) FE_{CO} and (c) CO J_p for all catalysts at different applied voltages. (d) FE_{H_2} and (e) FE_{CO} for PABA-, PSBA-, and PSABA-modified TCPP(Co)/Zr-BTB at different potentials. Reproduced with permission.[18] Copyright (2019) Wiley-VCH.

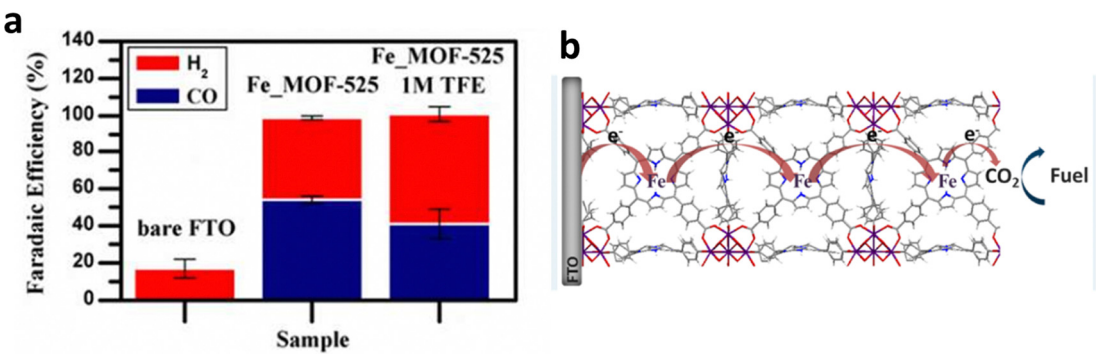

Fig. 19 (a) FE over approximately 4 h of bare FTO, Fe_MOF-525 with/without 2,2,2-trifluoroethanol (TFE). (b) Proposed ECR mechanism on the Fe porphyrin-based MOF. Reproduced with permission.[22] Copyright (2015) American Chemical Society.

abundant nanoscale porosity of MOFs is also conducive for solvents, reactants, and electrolytes to access catalytic sites. Fe-TPP anchored on the metal nodes of MOF-525 serves as both an electrocatalyst and a redox-hopping conduit for transporting reduction equivalents to catalytic sites beneath the surface of the electrode.

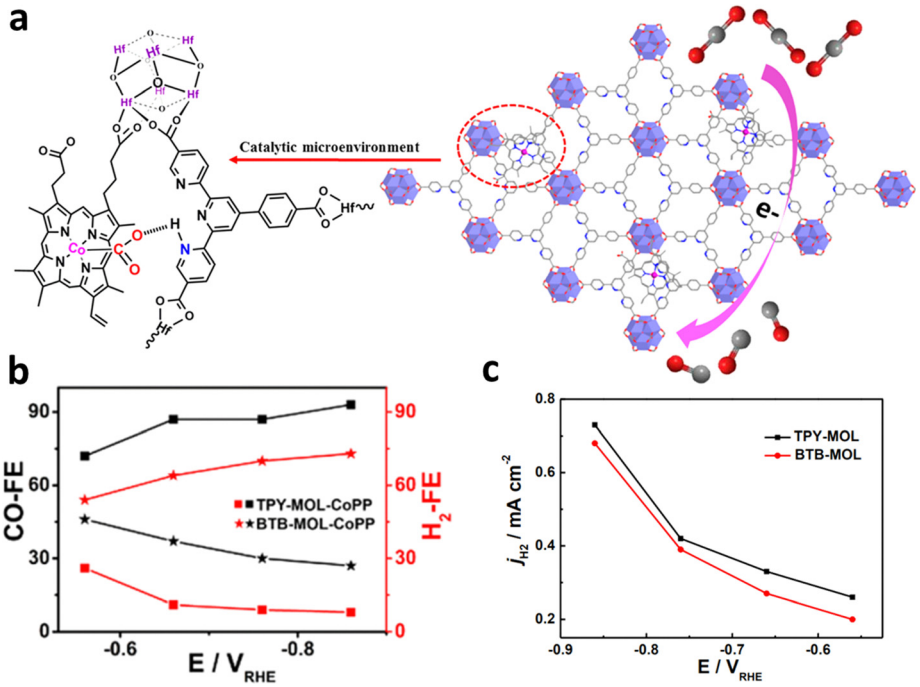

Fig. 20 (a) Schematic diagram of TPY-MOL-CoPP and the synergetic role of two different moieties (CoPP and TPY) for ECR. (b) FE_{CO} and FE_{H_2} as well as (c) HER current density for TPY- and BTB-MOL-CoPP. Reproduced with permission.[122] Copyright (2019) American Chemical Society.

5.2. SSCs located in ligands

Single-site metal atoms can also be designed in the ligands of MOFs.[121] Through ingenious design of ligands, different binding sites (*i.e.* N, O, P, and S) can be incorporated in ligands to anchor single-atomic metal in the MOFs. Therefore, choosing a ligand with appropriate binding sites is critical for the incorporation of single-site active sites into MOFs. Wang *et al.* prepared cobalt protoporphyrin (CoPP) installed on 4′-(4-benzoate)-(2,2′,2″-terpyridine)-5,5″-dicarboxylate (TPY) and BTB on metal–organic layers (MOLs) as SSCs.[122] Both the pyridinium group and CoPP on the TPY linkers could activate CO_2 by constructing [pyH^+–^-O_2C–CoPP] adducts when these catalysts were applied for the ECR, which enhances the ECR activity and inhibit the HER process (Fig. 20a). After 1 e^- reduction of CoPP, CO_2 is adsorbed and transferred to $[HO_2C–CoPP]^0$, which competes with $[H–CoPP]^0$ which prefers the HER. The ECR is more favorable than the HER pathway in the catalysts because the pre-assembled pyridine moiety stabilizes the $[pyHO_2C–CoPP]^0$ clusters, resulting in a higher CO/H_2 selectivity than BTB-MOL-CoPP (Fig. 20b). Moreover, the synergistic stabilization effect from the [pyH^+–^-O_2C–CoPP] resulted in a high selectivity for CO production at around −0.9 V, corresponding to a high TOF (0.4 s^{-1}). As shown in Fig. 20c, only HER activity was observed when the same test was carried out using catalysts (TPY-MOL and BTB-MOL) without CoPP, indicating that CoPP is the dominant active sites for ECR.

Lan *et al.* synthesized polyoxometalate–metalloporphyrin organic frameworks (PMOFs) coordinated by M-TCPP linkers (tetrakis[4-carboxyphenyl]-porphyrin-M) and reductive Zn-ε-Keggin clusters *via* a hydrothermal method.[123] The obtained PMOFs had the general formula $[PMo_8^{V}Mo_4^{VI}O_{35}(OH)_5Zn_4]_2$[M-TCPP][$2H_2O$][1.5TBAOH] (M = Fe, Co, Ni, and Zn, TBAOH = tetrabutylammonium hydroxide) (Fig. 21a). In this structure, the four Zn-ε-Keggin chains were assembled by M-TCPP *via* the coordination connection between the carboxyl group and Zn clusters. M-TCPP and Zn clusters both served as electron donors and ECR active sites (Fig. 21b). The PMOFs demonstrated excellent performance in ECR, especially for the Co-PMOF, achieving a high FE_{CO} of 99%, a high TOF (nearly 1700 h^{-1}), and robust stability over 35 h (Fig. 21c).

5.3. SSCs located in nanopores

Tunable nanopores in MOFs can also be used to anchor single-site atoms of appropriate size. Lan *et al.* implanted metallocene (MCp_2, Cp stands for cyclopentadienyl, M = Fe, Ni, Co) into the pores of metalloporphyrin-based MOF-545 *via* chemical vapor deposition by taking advantage of the high porosity, large pore size, and excellent physical/chemical stability of MOF-545 (Fig. 22a).[21] Furthermore, experiments and DFT calculations revealed that in the obtained MCp_2@MOF-545 composite material, the π-electron cyclopentadienyl ring system might be overlapped with the π-electron system of porphyrin. In addition, MCp_2 can be used as an electron donor and carrier to form a continuous electron transport channel in MOF-545. In addition, the strong binding interaction with metalloporphyrin in the ECR process greatly reduces the adsorption energy of CO_2, thus enhancing ECR activity (Fig. 22b). $CoCp_2$@-MOF-545-Co (97% at −0.7 V), $FeCp_2$@MOF-545-Co (94.1%, at −0.8 V), and $NiCp_2$@MOF-545-Co (82.6%, at −0.8 V) all exhibited high FE_{CO} specifically (Fig. 22c). The loading of single

active sites into the nanopores of MOFs opens up new possibilities to promote the ECR process and inspires the development of high-selectivity ECR electrocatalysts.

SSCs anchored on MOFs have various adjustable properties because of their adjustable structure and porosity. Furthermore, they have become an important research topic for ECR. However, they also face many challenges: (1) the introduction of single-site active centers in MOFs, either in the pores or anchored on the metal nodes, may hinder the mass transfer process. (2) It is difficult to achieve precise control of catalysts and high single-site metal loading because of the mutual restriction of MOFs and single-site active centers. (3) It is difficult to achieve precise positioning and structural analysis of single-site catalysts because of the limited characterization technology. Therefore, efforts should be dedicated to developing more *in situ* and *ex situ* spectroscopic characterizations as well as theoretical simulations and calculations. Only in this way can we realize the precise control of SSC-anchored MOFs and unlock their great potential for ECR.

6. COF-supported single-site catalysts

COFs are entirely made up of light elements linked together by strong covalent bonds, and are extensively applied in gas transportation and conversion because of their numerous pores and interfaces that interact with gas molecules.[124–126] Moreover, COFs have been considered a promising platform for supporting SSCs for ECR because of their permanent porosity and tunable building blocks, which are conducive to the adsorption and diffusion of CO_2.

By incorporating metal macrocyclic units (such as porphyrin,[127] phthalocyanine[128] *etc.*), the advantages of both molecular (high ECR selectivity) and heterogeneous catalysts (stable in water) can be

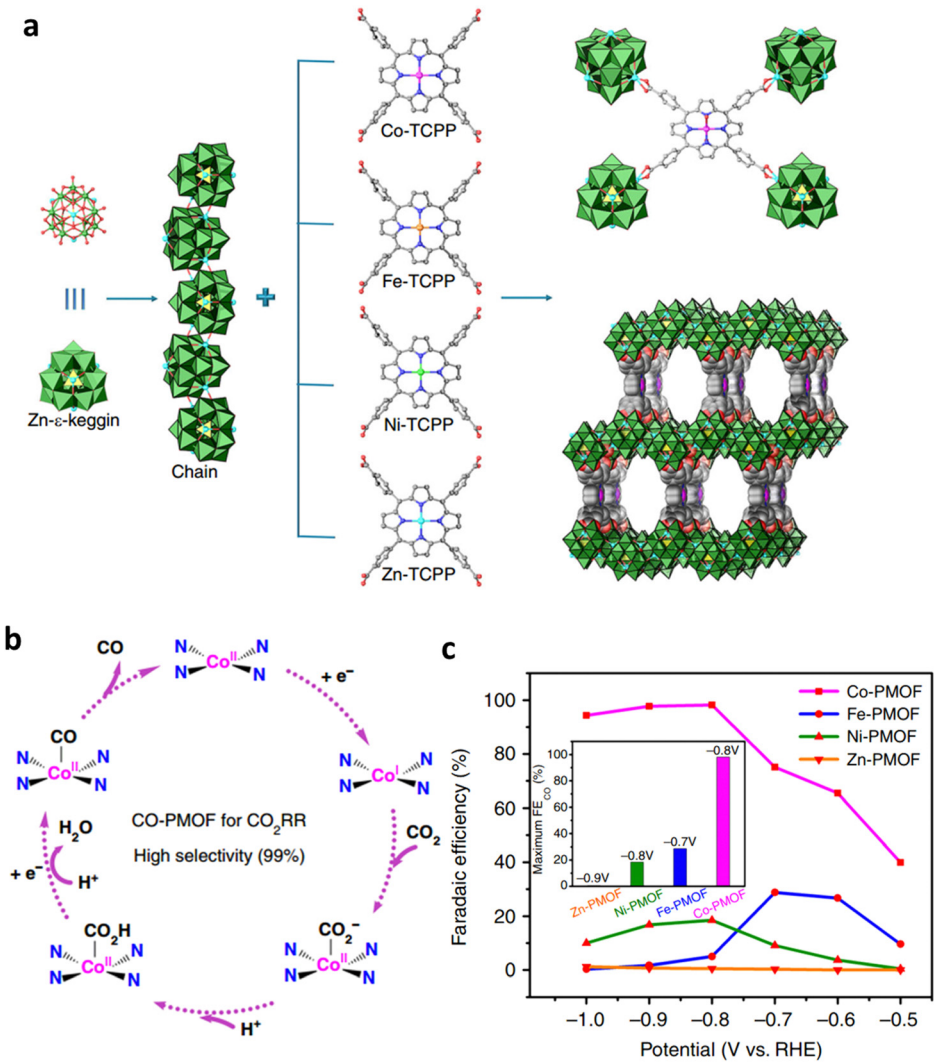

Fig. 21 (a) Structural diagram of M-PMOFs. (b) Proposed ECR mechanism on Co-PMOF. (c) FE_{CO} of M-PMOFs. Reproduced with permission.[123] Copyright (2018) Springer Nature.

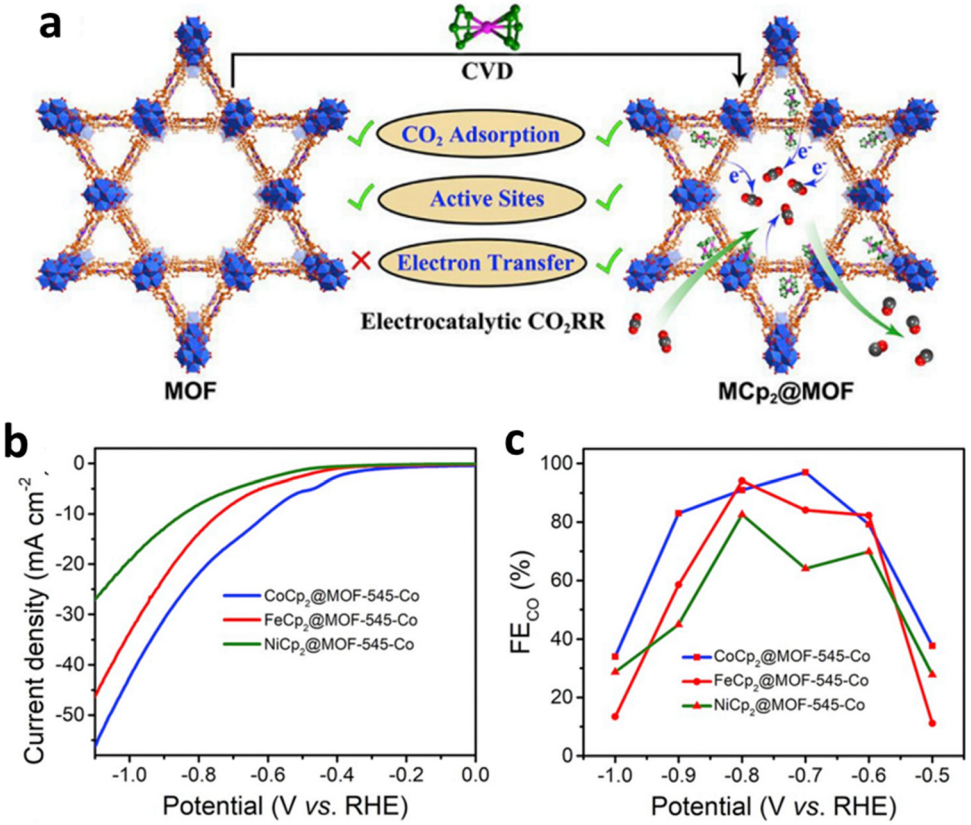

Fig. 22 (a) The comparison of MCp_2@MOF and MOF in ECR. (b) LSV and (c) FE_{CO} for MCp_2@MOF-545-Co. Reproduced with permission.[21] Copyright (2020) Elsevier Ltd.

achieved simultaneously in the obtained COFs. For instance, by using imine bonds to link cobalt porphyrin catalysts and organic struts, Yaghi and his co-workers reported a modular optimization strategy of COFs for ECR (Fig. 23a).[129] The covalent coordination of cobalt porphyrin within a COF was shown to affect the ECR mechanism in electrochemical experiments. The as-obtained COF-367-Co catalyst showed a high FE_{CO} (90%), a high turnover number of nearly 300 000, and an impressive TOF of approximately 9400 h^{-1} under neutral conditions (Fig. 23b and c).

COFs constructed by amine bonds have also received increasing attention for ECR applications because of their robust stability in aqueous electrolytes. Deng *et al.* synthesized COF-300-AR and COF-366-M-AR with amine linkages with both 3D and 2D structures by reducing the COFs with imine linkers.[24] Spectroscopic results confirmed that the synergetic effect of the COFs and the Ag electrode at their interface was responsible for the enhanced ECR performance (Fig. 24a). In addition, the amine linkage showed a robust structure in 6 M HCl and 6 M NaOH (Fig. 24b). In particular, the COF-300-AR deposited on Ag electrode promoted the ECR with a FE_{CO} of 80% at −0.85 V and 53% at −0.7 V (Fig. 24c).

In general, COF-supported SSCs have unique advantages for studying the structure–performance relationship because of their regular pores, adjustable pore sizes, high surface areas, and high adjustability. The activity and selectivity of ECR can also be enhanced by introducing different building blocks into the COFs. However, COF-supported SSCs also face many challenges: (1) the synthesis and collection of COFs are complicated and costly, which limits their large-scale synthesis. In addition, the good dynamic covalent nature of C=N and B–O would also result in stability issues, limiting their application under harsh conditions. (2) The conductivity of the COFs is in the range of insulators and semiconductors. Further improvement in its electrical conductivity is of great significance for electrocatalysis. (3) The current ECR performance of COF-supported SSCs remains limited. Therefore, it is desirable to improve intrinsic ECR performance and selectivity. More research is needed to determine the exact structure-ECR performance relationship of COF-supported SSCs, which is beneficial for further performance optimization. As technology grows by leaps and bounds, COF-supported SSCs with high ECR performance may play a more significant role in the future.

7. Conclusion and perspective

ECR is critical for promoting the carbon cycle and reducing the greenhouse effect. Owing to their highly adjustable structure and clear active center, SSCs, including SACs, HMCs, MOF-supported SSCs, and COF-supported SSCs, have attracted substantial attention in ECR studies. The topic of emerging SSCs

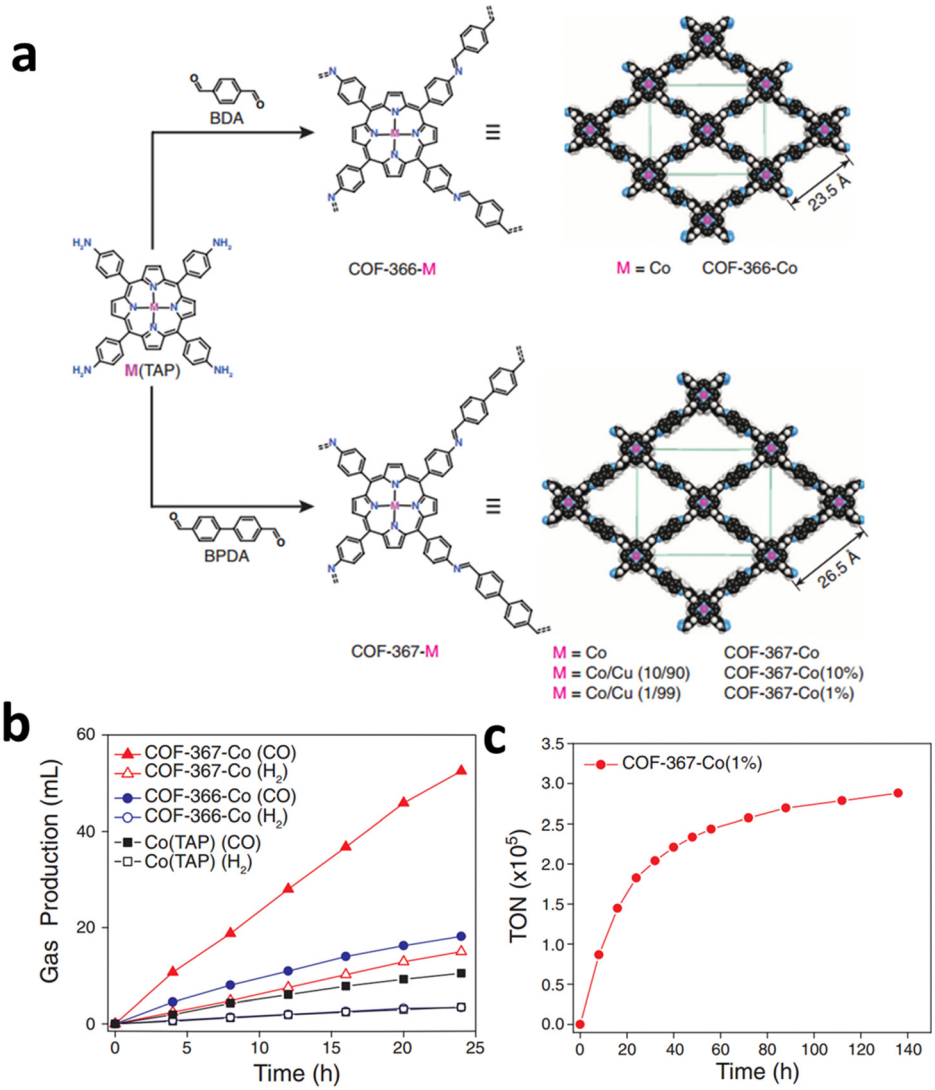

Fig. 23 (a) Design of metalloporphyrin-based COFs. (b) Long-term electrolysis at −0.67 V and gas production of different Co COFs catalysts. (c) Stability test and TON of Co COFs catalysts at −0.67 V. Reproduced with permission.[129] Copyright (2015) American Association for the Advancement of Science.

for ECR was comprehensively discussed in this review by investigating the reaction mechanisms, synthetic tactics, and optimization methods. We also summarized the typical examples from recent years to discuss the merits and shortcomings of SSCs for ECR (Table 1). In addition, we discussed solutions for these challenges, including the various obstacles and prospects in the application of these emerging SSCs. Although many achievements have already been made, further research is required to realize the industrialization of SSCs for ECR.

(1) Conducting in-depth fundamental research on basic catalyst theory

Theoretical knowledge on electrochemistry, surface chemistry, materials science, and simulation and calculations is the basis for the development of ECR science, which is an interdisciplinary subject. The structure and performance of SSCs are significantly affected by their coordination structures. An in-depth understanding of the chemistry involved in the design of more effective and stable catalysts can be achieved by more comprehensively studying the controllable structural characteristics of SSCs and the relationship between their coordination structure and performance.

(2) Exploring a low-cost and highly controllable synthetic strategy

Although numerous studies on SSCs have been conducted in the past decade, further research is required before SSCs can be used for practical applications. In addition, owing to the limitations of the synthesis method, SSCs are usually composed of particles. Therefore, SSCs with specific morphologies, more active sites, high surface areas, and high stability must be fabricated by using a highly controllable method. In addition, to realize the commercialization and large-scale application of SSCs, issues such as cost and environmental protection should be considered in these synthesis methods.

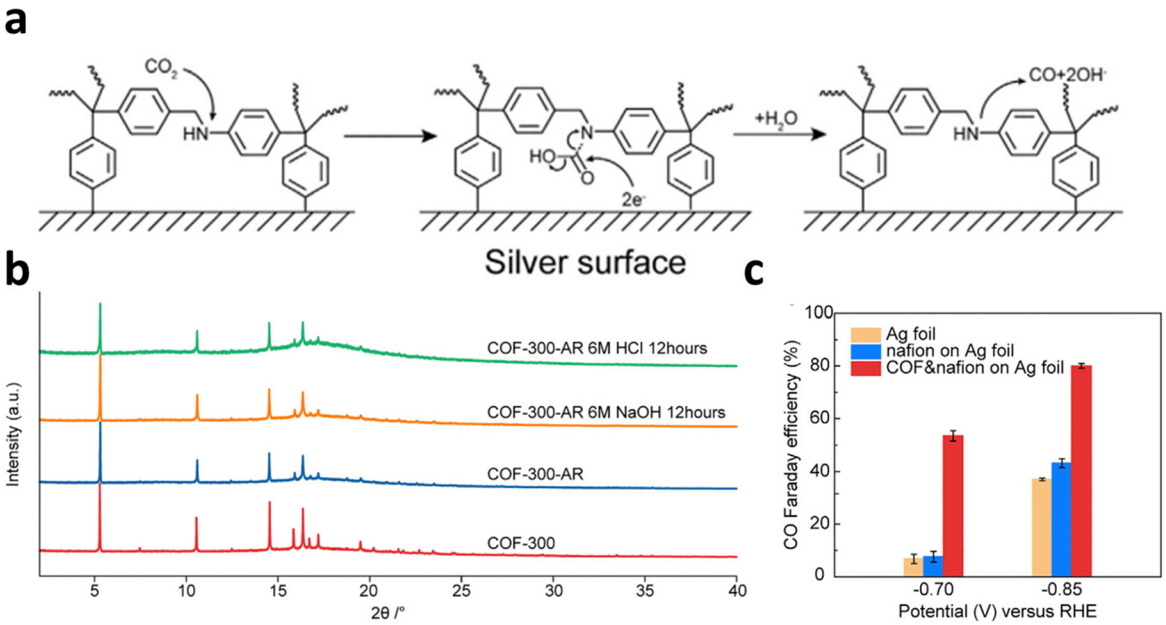

Fig. 24 (a) Schematic diagram of ECR at the interface of electrode. (b) XRD of COFs samples in HCl or NaOH solution. (c) FE_{CO} of the different COFs electrodes at −0.70 V and −0.85 V. Reproduced with permission.[24] Copyright (2018) Elsevier Ltd.

(3) Developing more practical applications

In addition to the impacts of catalysts, the ECR reaction highly depends on the conditions of the external equipment, such as the electrolyte (anion/cation species, concentration, pH, and phase state), ion-exchange membrane (cation-exchange/anion-exchange/bipolar membrane), electrolytic cells (H cells and

Table 1 Summary of the Catalytic Performance of SSCs toward ECR

Catalyst	Main product	Maximum FE	Reaction condition	Ref.
[a]Bi SACs	CO	97% (−0.5 V, j_p = 3.9 mA cm^{-2})	H-cell, 0.1 M $NaHCO_3$	130
[a]Co SACs	CO	97% (−0.6 V, j_p ≈ 22.5 mA cm^{-2})	H-cell, 0.1 M $KHCO_3$	131
[a]Ni SACs	CO	~99% (−0.681 V, j_p = 100 mA cm^{-2})	H-cell, 0.5 M $KHCO_3$	50
[a]Pd–NC	CO	55% (−0.5 V, j_p ≈ 0.57 mA cm^{-2})	H-cell, 0.5 M $NaHCO_3$	132
[a]Cu SACs	CH_3OH, CO	44% (methanol, −0.9 V, j_{tol} ≈ 90 mA cm^{-2}); 56% (CO, −0.9 V, j_{tol} ≈ 90 mA cm^{-2})	H-cell, 0.1 M $KHCO_3$	47
[a]Ni-SAC-2.5	CO	98.9% (−1.2 V, j_{tol} ≈ 7.5 mA cm^{-2})	H-cell, 0.1 M $KHCO_3$	133
[a]Fe–NC	CO	93% (~−0.6 V, j_p = 2.8 mA cm^{-2})	H-cell, 0.1 M $KHCO_3$	72
[a]Cu–CeO_2-4%	CH_4	~58% (−1.8 V, j_{tol} = 70 mA cm^{-2})	H-cell, 0.1 M $KHCO_3$	54
[b]CuPc	CH_4	~66% (−1.06 V, j_p = 13 mA cm^{-2})	H-cell, 0.5 M $KHCO_3$	134
[b]NiTAPc	CO	99% (~−0.74 V, j_{tol} = 32.3 mA cm^{-2})	H-cell, 0.5 M $KHCO_3$	135
[b]CoPc-Pyr	CO	95% (−0.7 V, j_{tol} = 2.5 mA cm^{-2})	H-cell, 0.05 M K_2CO_3	136
[b]Cr-bipyridine based HMCs	CO	~96% (−2.1 V *vs.* Fc^+/Fc)	H-cell, 0.1 M $TBAPF_6$/DMF, 0.62 M PhOH	137
[b]Mn-bipyridine based HMCs	HCOOH	90% (−1.77 V *vs.* Fc^+/Fc)	H-cell, 0.2 M Bu_4NBF_4/MeCN, 2.0 M TFE	138
[b]Ni-complexes	CO	87% (−2.44 V *vs.* $Fc^{+/0}$)	3-Neck pear-shaped glass cell, 0.1 M Bu_4NBF_4/CH_3CN	139
[b]Re-bipyridine based HMCs	CO	81% (−2.8 V *vs.* $Fc^{0/+}$)	H-cell, MeCN (0.1 M [nBu$_4$N][PF_6])	140
[b]Cu-porphyrin based HMCs	CH_4+ C_2H_2	44% (−0.976 V, j_p = 13.2 + 8.4 mA cm^{-2})	H-cell, 0.5 M $KHCO_3$	141
[c]Cu_2(CuTCPP)	HCOOH	68.4% (−1.55 V *vs* Ag/Ag^+, j_p ≈ 3 mA cm^{-2})	H-cell, 1 M H_2O and 0.5 M $EMIMBF_4$	142
[c]Co-MOF	CO	98.7% (−0.8 V, j_p = 18.8 mA cm^{-2})	H-cell, 0.5 M $KHCO_3$	123
[c]MOL-CoPP	CO	92.2% (−0.86 V, j_p = 1314 mA mg^{-1})	H-cell, 0.1 M $NaHCO_3$	122
[c]$CoCp_2$@MOF-545-Co	CO	97% (−0.7 V j_p = 15 mA cm^{-2})	H-cell, 0.5 M $KHCO_3$	21
[c]TCPP(Co)/Zr-BTB-PSABA	CO	85.1% (−0.769 V, j_{tol} = 6 mA cm^{-2})	H-cell, 0.5 M $KHCO_3$	143
[c]PcCu–O_8–Zn	CO	88% (−0.7 V, j_p = 2.5 mA cm^{-2})	H-cell, 0.1 M $KHCO_3$	143
[d]COF-366-Co	CO	90% (-0.67 V, j_p ≈ 80 mA mg^{-1})	0.2 M K_2HPO_4 buffer, 0.5 M $KHCO_3$	23
[d]Co-porphyrin based COF	CO	95% (−0.7 V, j_p ≈ 4.5 mA cm^{-2})	H-cell, 0.5 M $KHCO_3$	127
[d]COF-300-AR	CO	80% (−0.85 V)	H-cell, 0.1 M $KHCO_3$	24
[d]Co-porphyrin based COF	CO	95% (−0.6 V)	3-Compartment cell, 0.5 $KHCO_3$	144
[d]COF-366-Co	CO	87% (−0.67 V, 65 mA mg^{-1})	H-cell, 0.5 $KHCO_3$	145
[d]Fe-porphyrin based COF	CO	~80% (−2.2 V *vs.* Ag/AgCl)	One-compartment cell, 0.5 M TFE/MeCN	146

Note. a, b, c and d indicate that catalysts are SACs, HMCs, MOF-supported SSCs and COF-supported SSCs, respectively. j_p means partial current density, and j_{tol} means total current density.

flow cells), and gas diffusion electrodes. Therefore, more practical devices should be developed to adapt to different situations for ECR and promote the practical use of SSCs.

(4) Clarifying the catalytic mechanism through *in situ*/*ex situ* characterization and theoretical calculations

ECR is a reaction involving multiple electrons. In particular, the isolated active center atoms of the SSCs make the ECR mechanisms different from those of traditional bulk catalysts. Thus, the combination of *in situ*/*ex situ* characterizations and DFT calculations are helpful for in-depth observations and study of the surface reconstruction, ion diffusion, and electronic behavior of the catalyst during the reaction process and for the study of the specific reaction behavior of the intrinsic catalytic site. The SSC design and ECR mechanism can be understood by performing more advanced characterizations and well-developed calculations.

Conflicts of interest

There are no conflicts to declare.

Acknowledgements

This work was supported by the National Key Research and Development Program of China (2020YFA0715000), the National Natural Science Foundation of China (52127816, 51832004), the China Postdoctoral Science Foundation (2022T150502), National Energy-Saving and Low-Carbon Materials Production and Application Demonstration Platform Program (TC220H06N), and Hainan Provincial Joint Project of Sanya Yazhou Bay Science and Technology City (2021CXLH0007).

Notes and references

1 F. W. Li, A. Thevenon, A. Rosas-Hernández, Z. Y. Wang, Y. L. Li, C. M. Gabardo, A. Ozden, C. T. Dinh, J. Li, Y. H. Wang, J. P. Edwards, Y. Xu, C. McCallum, L. Z. Tao, Z. Q. Liang, M. C. Luo, X. Wang, H. H. Li, C. P. O'Brien, C. S. Tan, D. H. Nam, R. Quintero-Bermudez, T. T. Zhuang, Y. G. C. Li, Z. J. Han, R. D. Britt, D. Sinton, T. Agapie, J. C. Peters and E. H. Sargent, *Nature*, 2020, **577**, 509–513.
2 F. P. G. de Arquer, C. T. Dinh, A. Ozden, J. Wicks, C. McCallum, A. R. Kirmani, D. H. Nam, C. Gabardo, A. Seifitokaldani, X. Wang, Y. G. C. Li, F. W. Li, J. Edwards, L. J. Richter, S. J. Thorpe, D. Sinton and E. H. Sargent, *Science*, 2020, **367**, 661.
3 S. Ren, D. Joulie, D. Salvatore, K. Torbensen, M. Wang, M. Robert and C. P. Berlinguette, *Science*, 2019, **365**, 367–369.
4 W. Zhang, C. Huang, J. Zhu, Q. Zhou, R. Yu, Y. Wang, P. An, J. Zhang, M. Qiu, L. Zhou, L. Mai, Z. Yi and Y. Yu, *Angew. Chem., Int. Ed.*, 2022, **61**, e202112116.
5 K. P. Kuhl, E. R. Cave, D. N. Abram and T. F. Jaramillo, *Energy Environ. Sci.*, 2012, **5**, 7050–7059.
6 J. Qiao, Y. Liu, F. Hong and J. Zhang, *Chem. Soc. Rev.*, 2014, **43**, 631–675.
7 W. Zhang, C. Huang, Q. Xiao, L. Yu, L. Shuai, P. An, J. Zhang, M. Qiu, Z. Ren and Y. Yu, *J. Am. Chem. Soc.*, 2020, **142**, 11417–11427.
8 Y. Hori, A. Murata, R. Takahashi and S. Suzuki, *J. Am. Chem. Soc.*, 1987, **109**, 5022–5023.
9 J.-W. Chen, S.-H. Hsieh, S.-S. Wong, Y.-C. Chiu, H.-W. Shiu, C.-H. Wang, Y.-W. Yang, Y.-J. Hsu, D. Convertino, C. Coletti, S. Heun, C.-H. Chen and C.-L. Wu, *ACS Energy Lett.*, 2022, **7**, 2297–2303.
10 L. Chen, Z. Qi, X. Peng, J.-L. Chen, C.-W. Pao, X. Zhang, C. Dun, M. Young, D. Prendergast, J. J. Urban, J. Guo, G. A. Somorjai and J. Su, *J. Am. Chem. Soc.*, 2021, **143**, 12074–12081.
11 A. Iemhoff, M. Vennewald and R. Palkovits, *Angew. Chem., Int. Ed.*, 2023, **62**, e202212015.
12 X. Li, S. Feng, P. Hemberger, A. Bodi, X. Song, Q. Yuan, J. Mu, B. Li, Z. Jiang and Y. Ding, *ACS Catal.*, 2021, **11**, 9242–9251.
13 X. Liu, Z. Hao, H. Wang, T. Wang, Z. Shen, H. Zhang, S. Zhan and J. Gong, *Proc. Natl. Acad. Sci. U. S. A.*, 2022, **119**, e2119723119.
14 T. Shao, D. Duan, S. Liu, C. Gao, H. Ji and Y. Xiong, *Nanoscale*, 2022, **14**, 833–841.
15 J. Sheng, S. Sun, G. Jia, S. Zhu and Y. Li, *ACS Nano*, 2022, **16**, 15994–16002.
16 M. Zhang, H. Zhang, F. Li, W. Peng, L. Yao, Y. Dong, D. Xie, Z. Liu, C. Li and J. Zhang, *ACS Sustainable Chem. Eng.*, 2022, **10**, 13991–14000.
17 Q. He, D. Liu, J. H. Lee, Y. Liu, Z. Xie, S. Hwang, S. Kattel, L. Song and J. G. Chen, *Angew. Chem., Int. Ed.*, 2020, **59**, 3033–3037.
18 X. Zhang, S. Hou, J. Wu and Z. Gu, *Chem. – Eur. J.*, 2020, **26**, 1604–1611.
19 S. Roy, B. Sharma, J. Pécaut, P. Simon, M. Fontecave, P. D. Tran, E. Derat and V. Artero, *J. Am. Chem. Soc.*, 2017, **139**, 3685–3696.
20 T. H. T. Myren, A. Alherz, J. R. Thurston, T. A. Stinson, C. G. Huntzinger, C. B. Musgrave and O. R. Luca, *ACS Catal.*, 2020, **10**, 1961–1968.
21 Z. Xin, Y. Wang, Y. Chen, W. Li, L. Dong and Y. Lan, *Nano Energy*, 2020, **67**, 104233.
22 I. Hod, M. D. Sampson, P. Deria, C. P. Kubiak, O. K. Farha and J. T. Hupp, *ACS Catal.*, 2015, **5**, 6302–6309.
23 K.-Y. A. Lin and H.-A. Chang, *Chemosphere*, 2015, **139**, 624–631.
24 H. Liu, J. Chu, Z. Yin, X. Cai, L. Zhuang and H. Deng, *Chem*, 2018, **4**, 1696–1709.
25 W. Cheng, H. Su and Q. Liu, *Acc. Chem. Res.*, 2022, **55**, 1949–1959.
26 Q. Hao, Q. Tang, H.-X. Zhong, J.-Z. Wang, D.-X. Liu and X.-B. Zhang, *Sci. Bull.*, 2022, **67**, 1477–1485.
27 C. Long, K. Wan, X. Qiu, X. Zhang, J. Han, P. An, Z. Yang, X. Li, J. Guo, X. Shi, H. Wang, Z. Tang and S. Liu, *Nano Res.*, 2022, **15**, 1817–1823.

28 S. Gonell, M. D. Massey, I. P. Moseley, C. K. Schauer, J. T. Muckerman and A. J. M. Miller, *J. Am. Chem. Soc.*, 2019, **141**, 6658–6671.
29 W. Ju, A. Bagger, X. Wang, Y. Tsai, F. Luo, T. Moeller, H. Wang, J. Rossmeisl, A. Sofia Varela and P. Strasser, *ACS Energy Lett.*, 2019, **4**, 1663–1671.
30 C. W. Machan, S. A. Chabolla, J. Yin, M. K. Gilson, F. A. Tezcan and C. P. Kubiak, *J. Am. Chem. Soc.*, 2014, **136**, 14598–14607.
31 Y. Wang, S. L. Marquard, D. Wang, C. Dares and T. J. Meyer, *ACS Energy Lett.*, 2017, **2**, 1395–1399.
32 M. G. Kibria, J. P. Edwards, C. M. Gabardo, D. Caothang, A. Seifitokaldani, D. Sinton and E. H. Sargent, *Adv. Mater.*, 2019, **31**, 1807166.
33 S. Nitopi, E. Bertheussen, S. B. Scott, X. Liu, A. K. Engstfeld, S. Horch, B. Seger, I. E. L. Stephens, K. Chan, C. Hahn, J. K. Nørskov, T. F. Jaramillo and I. Chorkendorff, *Chem. Rev.*, 2019, **119**, 7610–7672.
34 L. Gong, D. Zhang, C. Lin, Y. Zhu, Y. Shen, J. Zhang, X. Han, L. Zhang and Z. Xia, *Adv. Energy Mater.*, 2019, **9**, 1902625.
35 G. Han, Y. Zheng, X. Zhang, Z. Wang, Y. Gong, C. Du, M. N. Banis, Y. Yiu, T. Sham, L. Gu, Y. Sun, Y. Wang, J. Wang, Y. Gao, G. Yin and X. Sun, *Nano Energy*, 2019, **66**, 104088.
36 B. Pattengale, Y. Huang, X. Yan, S. Yang, S. Younan, W. Hu, Z. Li, S. Lee, X. Pan, J. Gu and J. Huang, *Nat. Commun.*, 2020, **11**, 4114.
37 Q. Wang, X. Huang, Z. L. Zhao, M. Wang, B. Xiang, J. Li, Z. Feng, H. Xu and M. Gu, *J. Am. Chem. Soc.*, 2020, **142**, 7425–7433.
38 Z. Geng, Y. Liu, X. Kong, P. Li, K. Li, Z. Liu, J. Du, M. Shu, R. Si and J. Zeng, *Adv. Mater.*, 2018, **30**, 1803498.
39 B. Zhang, C. Zhu, Z. Wu, E. Stavitski, Y. H. Lui, T. Kim, H. Liu, L. Huang, X. Luan, L. Zhou, K. Jiang, W. Huang, S. Hu, H. Wang and J. S. Francisco, *Nano Lett.*, 2020, **20**, 136–144.
40 B. Qiao, A. Wang, X. Yang, L. F. Allard, Z. Jiang, Y. Cui, J. Liu, J. Li and T. Zhang, *Nat. Chem.*, 2011, **3**, 634–641.
41 L. Li, I. M. U. Hasan, Farwa, R. He, L. Peng, N. Xu, N. K. Niazi, J.-N. Zhang and J. Qiao, *Nano Res. Energy*, 2022, **1**, e9120015.
42 H. Guo, D.-H. Si, H.-J. Zhu, Q.-X. Li, Y.-B. Huang and R. Cao, *eScience*, 2022, **2**, 295–303.
43 J. Yang, R. Zhang, H. Zhao, H. Qi, J. Li, J.-F. Li, X. Zhou, A. Wang, K. Fan, X. Yan and T. Zhang, *Exploration*, 2022, **2**, 20210267.
44 Y. Yang, S. Wang, X. Tu, Z. Hu, Y. Zhu, H. Guo, Z. Li, L. Zhang, M. Peng, L. Jia, M. Yang, G. Yang, X. Qiao, J. Sun, X. Liang, Z. Zhang, Y. Zhu, L. Shi, C. Jiang, Y. Zhao, J. Li, Z. Shao, X. Zhang and Y. Sun, *Exploration*, 2022, **2**, 20220060.
45 X. Duan, J. Xu, Z. Wei, J. Ma, S. Guo, S. Wang, H. Liu and S. Dou, *Adv. Mater.*, 2017, **29**, 1701784.
46 C. Gao, S. Chen, Y. Wang, J. Wang, X. Zheng, J. Zhu, L. Song, W. Zhang and Y. Xiong, *Adv. Mater.*, 2018, **30**, 1704624.
47 H. Yang, L. Shang, Q. Zhang, R. Shi and T. Zhang, *Nat. Commun.*, 2019, **10**, 1–9.
48 T. Maiyalagan, X. Wang and H. Wang, *ACS Catal.*, 2012, **2**, 781–794.
49 Z. Ma, X. Zhang, D. Wu, X. Han, L. Zhang, H. Wang, F. Xu, Z. Gao and K. Jiang, *J. Colloid Interface Sci.*, 2020, **570**, 31–40.
50 T. Zheng, K. Jiang, N. Ta, Y. Hu, J. Zeng, J. Liu and H. Wang, *Joule*, 2019, **3**, 265–278.
51 X. Zu, X. Li, W. Liu, Y. Sun, J. Xu, T. Yao, W. Yan, S. Gao, C. Wang, S. Wei and Y. Xie, *Adv. Mater.*, 2019, **31**, 1808135.
52 X. Liu, Z. Wang, Y. Tian and J. Zhao, *J. Phys. Chem. C*, 2020, **124**, 3722–3730.
53 S. Zhao, Y. Cheng, J. Veder, B. Johannessen, M. Saunders, L. Zhang, C. Liu, M. F. Chisholm, R. De Marco, J. Liu, S. Yang and S. P. Jiang, *ACS Appl. Energy Mater.*, 2018, **1**, 5286–5297.
54 Y. Pan, R. Lin, Y. J. Chen, S. J. Liu, W. Zhu, X. Cao, W. X. Chen, K. L. Wu, W. C. Cheong, Y. Wang, L. R. Zheng, J. Luo, Y. Lin, Y. Q. Liu, C. G. Liu, J. Li, Q. Lu, X. Chen, D. S. Wang, Q. Peng, C. Chen and Y. D. Li, *J. Am. Chem. Soc.*, 2018, **140**, 4218–4221.
55 H. Fei, J. Dong, M. J. Arellano-Jiménez, G. Ye, N. Dong Kim, E. L. G. Samuel, Z. Peng, Z. Zhu, F. Qin, J. Bao, M. J. Yacaman, P. M. Ajayan, D. Chen and J. M. Tour, *Nat. Commun.*, 2015, **6**, 8668.
56 H. Fei, J. Dong, Y. Feng, C. S. Allen, C. Wan, B. Volosskiy, M. Li, Z. Zhao, Y. Wang, H. Sun, P. An, W. Chen, Z. Guo, C. Lee, D. Chen, I. Shakir, M. Liu, T. Hu, Y. Li, A. I. Kirkland, X. Duan and Y. Huang, *Nat. Catal.*, 2018, **1**, 63–72.
57 X. Zu, X. Li, W. Liu, Y. Sun and Y. Xie, *Adv. Mater.*, 2019, **31**, 1808135.
58 V. Tripkovic, M. Vanin, M. Karamad, M. E. Björketun, K. W. Jacobsen, K. S. Thygesen and J. Rossmeisl, *J. Phys. Chem. C*, 2013, **117**, 9187–9195.
59 A. S. Varela, N. Ranjbar Sahraie, J. Steinberg, W. Ju, H.-S. Oh and P. Strasser, *Angew. Chem., Int. Ed.*, 2015, **54**, 10758–10762.
60 A. S. Varela, W. Ju, A. Bagger, P. Franco, J. Rossmeisl and P. Strasser, *ACS Catal.*, 2019, **9**, 7270–7284.
61 Y. Cheng, S. Zhao, H. Li, S. He, J.-P. Veder, B. Johannessen, J. Xiao, S. Lu, J. Pan, M. F. Chisholm, S.-Z. Yang, C. Liu, J. G. Chen and S. P. Jiang, *Appl. Catal., B*, 2019, **243**, 294–303.
62 P. Su, K. Iwase, T. Harada, K. Kamiya and S. Nakanishi, *Chem. Sci.*, 2018, **9**, 3941–3947.
63 W. Zheng, J. Yang, H. Chen, Y. Hou, Q. Wang, M. Gu, F. He, Y. Xia, Z. Xia, Z. Li, B. Yang, L. Lei, C. Yuan, Q. He, M. Qiu and X. Feng, *Adv. Funct. Mater.*, 2020, **30**, 1907658.
64 X. Zhang, J. Guo, P. Guan, C. Liu, H. Huang, F. Xue, X. Dong, S. J. Pennycook and M. F. Chisholm, *Nat. Commun.*, 2013, **4**, 1924.
65 H. J. Qiu, Y. Ito, W. Cong, Y. Tan, P. Liu, A. Hirata, T. Fujita, Z. Tang and M. Chen, *Angew. Chem., Int. Ed.*, 2015, **54**, 14031–14035.

66 K. Jiang, T. T. Zheng, Y. F. Hu, S. Hwang, E. Stavitski, Y. D. Peng, J. Dynes, M. Gangisetty, D. Su, K. Attenkofer and H. T. Wang, *Energy & Environ. Sci.*, 2018, **11**(4), 893–903.
67 J. Liu, X. Kong, L. Zheng, X. Guo, X. Liu and J. Shui, *ACS Nano*, 2020, **14**, 1093–1101.
68 S. Abednatanzi, P. G. Derakhshandeh, H. Depauw, F. Coudert, H. Vrielinck, P. Van Der Voort and K. Leus, *Chem. Soc. Rev.*, 2019, **48**, 2535–2565.
69 S. Dissegna, K. Epp, W. R. Heinz, G. Kieslich and R. A. Fischer, *Adv. Mater.*, 2018, **30**, 1704501.
70 J. Li, W. Huang, M. Wang, S. Xi, J. Meng, K. Zhao, J. Jin, W. Xu, Z. Wang and X. Liu, *ACS Energy Lett.*, 2018, **4**, 285–292.
71 J. Gu, C.-S. Hsu, L. Bai, H. M. Chen and X. Hu, *Science*, 2019, **364**, 1091–1094.
72 F. Pan, H. Zhang, K. Liu, D. Cullen, K. More, M. Wang, Z. Feng, G. Wang, G. Wu and Y. Li, *ACS Catal.*, 2018, **8**, 3116–3122.
73 F. Pan, H. Zhang, Z. Liu, D. Cullen, K. Liu, K. More, G. Wu, G. Wang and Y. Li, *J. Mater. Chem. A*, 2019, **7**, 26231–26237.
74 H. Yang, Y. Wu, G. Li, Q. Lin, Q. Hu, Q. Zhang, J. Liu and C. He, *J. Am. Chem. Soc.*, 2019, **141**, 12717–12723.
75 X. Wang, Y. Pan, H. Ning, H. Wang, D. Guo, W. Wang, Z. Yang, Q. Zhao, B. Zhang, L. Zheng, J. Zhang and M. Wu, *Appl. Catal., B*, 2020, **266**, 118630.
76 C. Yuan, K. Liang, X. Xia, Z. Yang, Y. Jiang, T. Zhao, C. Lin, T. Cheang, S. Zhong and A. Xu, *Catal. Sci. Technol.*, 2019, **9**, 3669–3674.
77 J. K. Li, P. Pršlja, T. Shinagawa, A. J. M. Shinagawa, F. Krumeic, K. Artyushkova, P. Atanassov, A. Atanassov, Y. C. Zhou, R. García-Muelas, N. López, J. Pérez-Ramírez and F. Jaouen, *ACS Cat.*, 2019, **9**(11), 10426–10439.
78 X. Qin, S. Zhu, F. Xiao, L. Zhang and M. Shao, *ACS Energy Lett.*, 2019, **4**, 1778–1783.
79 X. Zhou, W. Yang, Q. Chen, Z. Geng, X. Shao, J. Li, Y. Wang, D. Dai, W. Chen, G. Xu, X. Yang and K. Wu, *J. Phys. Chem. C*, 2016, **120**, 1709–1715.
80 J. Lin, A. Wang, B. Qiao, X. Liu, X. Yang, X. Wang, J. Liang, J. Li, J. Liu and T. Zhang, *J. Am. Chem. Soc.*, 2013, **135**, 15314–15317.
81 X. Gu, B. Qiao, C. Huang, W. Ding, K. Sun, E. Zhan, T. Zhang, J. Liu and W. Li, *ACS Catal.*, 2014, **4**, 3886–3890.
82 P. Liu, Y. Zhao, R. Qin, S. Mo, G. Chen, L. Gu, D. M. Chevrier, P. Zhang, Q. Guo, D. Zang, B. Wu, G. Fu and N. Zheng, *Science*, 2016, **352**, 797–801.
83 S. E. J. Hackett, R. M. Brydson, M. H. Gass, I. Harvey, A. D. Newman, K. Wilson and A. F. Lee, *Angew. Chem., Int. Ed.*, 2007, **46**, 8593–8596.
84 J. S. Elias, K. A. Stoerzinger, W. T. Hong, M. Risch, L. Giordano, A. N. Mansour and Y. Shao-Horn, *ACS Catal.*, 2017, **7**, 6843–6857.
85 S. Bai, Q. Shao, P. Wang, Q. Dai, X. Wang and X. Huang, *J. Am. Chem. Soc.*, 2017, **139**, 6827–6830.
86 D. Gao, Y. Zhang, Z. Zhou, F. Cai, X. Zhao, W. Huang, Y. Li, J. Zhu, P. Liu, F. Yang, G. Wang and X. Bao, *J. Am. Chem. Soc.*, 2017, **139**, 5652–5655.
87 Y. Wang, Z. Chen, P. Han, Y. Du, Z. Gu, X. Xu and G. Zheng, *ACS Catal.*, 2018, **8**, 7113–7119.
88 S. Back and Y. Jung, *ACS Energy Lett.*, 2017, **2**, 969–975.
89 S. Yang, J. Kim, Y. J. Tak, A. Soon and H. Lee, *Angew. Chem., Int. Ed.*, 2016, **55**, 2058–2062.
90 Z. Liu, Y. Du, P. Zhang, Z. Zhuang and D. Wang, *Matter*, 2021, **4**, 3161–3194.
91 J. Wang, M. Yan, K. Zhao, X. Liao, P. Wang, X. Pan, W. Yang and L. Mai, *Adv. Mater.*, 2017, **29**, 1604464.
92 X. Pan, M. Yan, C. Sun, K. Zhao, W. Luo, X. Hong, Y. Zhao, L. Xu and L. Mai, *Adv. Funct. Mater.*, 2021, **31**, 2007840.
93 K. Chan, C. Tsai, H. A. Hansen and J. K. Nørskov, *ChemCatChem*, 2014, **6**, 1899–1905.
94 X. Hong, K. Chan, C. Tsai and J. K. Nørskov, *ACS Catal.*, 2016, **6**, 4428–4437.
95 L. S. Byskov, J. K. Nørskov, B. S. Clausen and H. Topsøe, *Catal. Lett.*, 2000, **64**, 95–99.
96 H. Li, L. Wang, Y. Dai, Z. Pu, Z. Lao, Y. Chen, M. Wang, X. Zheng, J. Zhu, W. Zhang, R. Si, C. Ma and J. Zeng, *Nat. Nanotechnol.*, 2018, **13**, 411–417.
97 Z. Lu, Y. Cheng, S. Li, Z. Yang and R. Wu, *Appl. Surf. Sci.*, 2020, **528**, 147047.
98 M. H. Ronne, D. Cho, M. R. Madsen, J. B. Jakobsen, S. Eom, E. Escoude, C. D. Hammershoj, D. U. Nielsen, S. U. Pedersen, M. Baik, T. Skrydstrup and K. Daasbjerg, *J. Am. Chem. Soc.*, 2020, **142**, 4265–4275.
99 Y. Wu, B. Rudshteyn, A. Zhanaidarova, J. D. Froehlich, W. Ding, C. P. Kubiak and V. S. Batista, *ACS Catal.*, 2017, **7**, 5282–5288.
100 L. Sun, V. Reddu, A. C. Fisher and X. Wang, *Energy Environ. Sci.*, 2020, **13**, 374–403.
101 N. Furuya and S. Koide, *Electrochim. Acta*, 1991, **36**, 1309–1313.
102 N. Furuya and K. Matsui, *J. Electroanal. Chem.*, 1989, **271**, 181–191.
103 Y. Y. Birdja, J. Shen and M. T. M. Koper, *Catal. Today*, 2017, **288**, 37–47.
104 A. J. Göttle and M. T. M. Koper, *J. Am. Chem. Soc.*, 2018, **140**, 4826–4834.
105 N. Corbin, J. Zeng, K. Williams and K. Manthiram, *Nano Res.*, 2019, **12**, 2093–2125.
106 C. Y. Ruan, V. Mastryukov and M. Fink, *J. Chem. Phys.*, 1999, **111**, 3035–3041.
107 N. Kaeffer, M. Chavarotkerlidou and V. Artero, *Acc. Chem. Res.*, 2015, **48**, 1286–1295.
108 J. Choi, P. Wagner, S. Gambhir, R. Jalili, D. R. MacFarlane, G. G. Wallace and D. L. Officer, *ACS Energy Lett.*, 2019, **4**, 666–672.
109 J. Wang, L. Gan, Q. Zhang, V. Reddu, Y. Peng, Z. Liu, X. Xia, C. Wang and X. Wang, *Adv. Energy Mater.*, 2019, **9**, 1803151.
110 Z. Weng, Y. Wu, M. Wang, J. Jiang, K. Yang, S. Huo, X. F. Wang, Q. Ma, G. W. Brudvig and V. S. Batista, *Nat. Commun.*, 2018, **9**, 415.
111 Z. Weng, J. Jing, Y. Wu, Z. Wu, X. Guo, K. L. Materna, W. Liu, V. S. Batista, G. W. Brudvig and H. Wang, *J. Am. Chem. Soc.*, 2016, **138**, 8076–8079.

112 S. Kusama, T. Saito, H. Hashiba, A. Sakai and S. Yotsuhashi, *ACS Catal.*, 2017, **7**, 8382–8385.
113 S. Liu, H. B. Yang, S. F. Hung, J. Ding and B. Liu, *Angew. Chem., Int. Ed.*, 2020, **59**, 798–803.
114 W. Huang, C. Chen, Z. Ling, J. Li, L. Qu, J. Zhu, W. Yang, M. Wang, K. A. Owusu, L. Qin, L. Zhou and L. Mai, *Chem. Eng. J.*, 2021, **405**, 126959.
115 J. Meng, X. Liu, C. Niu, Q. Pang, J. Li, F. Liu, Z. Liu and L. Mai, *Chem. Soc. Rev.*, 2020, **49**, 3142–3186.
116 W. Zhao, G. Li and Z. Tang, *Nano Today*, 2019, **27**, 178–197.
117 Y.-N. Gong, L. Jiao, Y. Qian, C.-Y. Pan, L. Zheng, X. Cai, B. Liu, S.-H. Yu and H.-L. Jiang, *Angew. Chem., Int. Ed.*, 2020, **59**, 2705–2709.
118 L. Jiao, W. Yang, G. Wan, R. Zhang, X. Zheng, H. Zhou, S.-H. Yu and H.-L. Jiang, *Angew. Chem., Int. Ed.*, 2020, **59**, 20589–20595.
119 Y. Zhang, L. Jiao, W. Yang, C. Xie and H.-L. Jiang, *Angew. Chem., Int. Ed.*, 2021, **60**, 7607–7611.
120 I. S. Kim, J. Borycz, A. E. Platero-Prats, S. Tussupbayev, T. C. Wang, O. K. Farha, J. T. Hupp, L. Gagliardi, K. W. Chapman, C. J. Cramer and A. B. F. Martinson, *Chem. Mater.*, 2015, **27**, 4772–4778.
121 K. K. Tanabe, C. A. Allen and S. M. Cohen, *Angew. Chem., Int. Ed.*, 2010, **49**, 9730–9733.
122 Y. Guo, W. Shi, H. Yang, Q. He, Z. Zeng, J.-Y. Ye, X. He, R. Huang, C. Wang and W. Lin, *J. Am. Chem. Soc.*, 2019, **141**, 17875–17883.
123 Y. Wang, Q. Huang, C. He, Y. Chen, J. Liu, F. Shen and Y. Lan, *Nat. Commun.*, 2018, **9**, 4466.
124 D. D. Medina, T. Sick and T. Bein, *Adv. Energy Mater.*, 2017, **7**, 1700387.
125 S. Royuela, R. Gil-San Millan, M. J. Mancheno, M. Mar Ramos, J. L. Segura, J. A. R. Navarro and F. Zamora, *Materials*, 2019, **12**, 1974.
126 H. Xu, S. Tao and D. Jiang, *Nat. Mater.*, 2016, **15**, 722.
127 Q. Wu, R. Xie, M. Mao, G. Chai, J. Yi, S. Zhao, Y. Huang and R. Cao, *ACS Energy Lett.*, 2020, **5**, 1005–1012.
128 C. Yao, J. Li, W. Gao and Q. Jiang, *Chem. – Eur. J.*, 2018, **24**, 11051–11058.
129 S. Lin, C. S. Diercks, Y.-B. Zhang, N. Kornienko, E. M. Nichols, Y. Zhao, A. R. Paris, D. Kim, P. Yang, O. M. Yaghi and C. J. Chang, *Science*, 2015, **349**, 1208–1213.
130 E. Zhang, T. Wang, K. Yu, J. Liu, W. Chen, A. Li, H. Rong, R. Lin, S. Ji, X. Zheng, Y. Wang, L. Zheng, C. Chen, D. Wang, J. Zhang and Y. Li, *J. Am. Chem. Soc.*, 2019, **141**, 16569–16573.
131 H. Yang, Q. Lin, Y. Wu, G. Li, Q. Hu, X. Chai, X. Ren, Q. Zhang, J. Liu and C. He, *Nano Energy*, 2020, **70**, 104454.
132 Q. He, J. H. Lee, D. Liu, Y. Liu, Z. Lin, Z. Xie, S. Hwang, S. Kattel, L. Song and J. G. Chen, *Adv. Funct. Mater.*, 2020, **30**, 2000407.
133 H. Yang, L. Shang, Q. Zhang, R. Shi, G. I. N. Waterhouse, L. Gu and T. Zhang, *Nat. Commun.*, 2019, **10**, 4585.
134 Z. Weng, Y. Wu, M. Wang, J. Jiang, K. Yang, S. Huo, X. Wang, Q. Ma, G. W. Brudvig, V. S. Batista, Y. Liang, Z. Feng and H. Wang, *Nat. Commun.*, 2018, **9**, 415.
135 S. Liu, H. B. Yang, S.-F. Hung, J. Ding, W. Cai, L. Liu, J. Gao, X. Li, X. Ren, Z. Kuang, Y. Huang, T. Zhang and B. Liu, *Angew. Chem., Int. Ed.*, 2020, **59**, 798–803.
136 A. De Riccardis, M. Lee, R. V. Kazantsev, A. J. Garza, G. Zeng, D. M. Larson, E. L. Clark, P. Lobaccaro, P. W. W. Burroughs, E. Bloise, J. W. Ager, A. T. Bell, M. Headgordon, G. Mele and F. M. Toma, *ACS Appl. Mater. Interfaces*, 2020, **12**, 5251–5258.
137 S. L. Hooe, J. M. Dressel, D. A. Dickie and C. W. Machan, *ACS Catal.*, 2020, **10**, 1146–1151.
138 M. H. Rønne, D. Cho, M. R. Madsen, J. B. Jakobsen, S. Eom, É. Escoudé, H. C. D. Hammershøj, D. U. Nielsen, S. U. Pedersen, M. Baik, T. Skrydstrup and K. Daasbjerg, *J. Am. Chem. Soc.*, 2020, **142**, 4265–4275.
139 X. Su, K. M. McCardle, J. A. Panetier and J. W. Jurss, *Chem. Commun.*, 2018, **54**, 3351–3354.
140 D. A. Popov, J. M. Luna, N. M. Orchanian, R. Haiges, C. A. Downes and S. C. Marinescu, *Dalton Trans.*, 2018, **47**, 17450–17460.
141 Z. Weng, J. Jiang, Y. Wu, Z. Wu, X. Guo, K. L. Materna, W. Liu, V. S. Batista, G. W. Brudvig and H. Wang, *J. Am. Chem. Soc.*, 2016, **138**, 8076–8079.
142 J. Wu, S. Hou, X. Zhang, M. Xu, H. Yang, P. Cao and Z. Gu, *Chem. Sci.*, 2019, **10**, 2199–2205.
143 H. Zhong, M. Ghorbani-Asl, K. H. Ly, J. Zhang, J. Ge, M. Wang, Z. Liao, D. Makarov, E. Zschech, E. Brunner, I. M. Weidinger, J. Zhang, A. V. Krasheninnikov, S. Kaskel, R. Dong and X. Feng, *Nat. Commun.*, 2020, **11**, 1409.
144 M. Zhu, D. Yang, R. Ye, J. Zeng, N. Corbin and K. Manthiram, *Catal. Sci. Technol.*, 2019, **9**, 974–980.
145 C. S. Diercks, S. Lin, N. Kornienko, E. A. Kapustin, E. M. Nichols, C. Zhu, Y. Zhao, C. J. Chang and O. M. Yaghi, *J. Am. Chem. Soc.*, 2018, **140**, 1116–1122.
146 P. L. Cheung, S. K. Lee and C. P. Kubiak, *Chem. Mater.*, 2019, **31**, 1908–1919.